MACQUARIE University
SYDNEY·AUSTRALIA

Department of Molecular Sciences

# Release properties of melatonin loaded mesoporous silica materials

*Irene Moroni*

9th October 2017

# Table of Contents

# Declaration

I declare that all the work presented in this thesis is my original research work, part of the Master of Research program at Macquarie University. The contents of this thesis has not been submitted for any type of degree or award at any other university previously. Wherever contributions of others were needed, every effort was made to indicate this clearly through references to the literature and acknowledgement of assistance or advice.

Irene Moroni

# Acknowledgements

I am grateful to Macquarie University for financial support through a Master of Research Scholarship and for a maintenance grant from the Department of Molecular Sciences. The Centre of Excellence for Nanoscale BioPhotonics (CNBP) provided access to the a PC2 laboratory where cell culture studies were conducted, which was very much appreciated. I am grateful too for access and support to Macquarie University's Microscopy Unit, as well as the Microscopy unit at UTS which provided access to and support in the collection of X-ray diffractograms.

I would like to thank all the people that helped me and supported me during this year. Thanks to my supervisor Dr. Alfonso Garcia-Bennett for teaching me the basis of mesoporous silica materials chemistry and giving me the opportunity to learn how to work in a more independent way. Thanks to my co-supervisor Dr. Maria Comas Soberats for patiently explaining me the basic of the biology connected with melatonin and cell culture and reassuring me in some critical moments. I want to acknowledge also Dr. Lindsay Parker for helping me in the biology lab and for her encouragements that comforted me more than once.

Thanks to my mother and my step-father for their constant support and unconditional love. Thanks to my Italian friends, in particular Carolina and Martina, for motivating me and cheering me up when needed. Thanks to all my friends in Australia for all their kind words, the laughs and the special moments we shared together.

# Abstract

Melatonin is a hormone produced by the pineal gland and involved in the regulation of circadian rhythms (e.g. sleep/wake cycle). Exogenous melatonin is used in the treatment of circadian disorders (e.g. delayed sleep phase syndrome, jet-lag or shift-work). In currently available commercial formulations melatonin has low bioavailability. Tailored formulations are needed to treat diverse and specific circadian disorders. Mesoporous silica materials can be efficient drug carriers as they are non-toxic biodegradable materials possessing high surface area, large pore volume and pore dimensions in the mesoscale range.

This study focused on the preparation of mesoporous silica formulations for controlling the release of melatonin. Mesoporous materials (MCM-41) were synthesised and characterized through different physicochemical techniques. They were loaded with melatonin and their release properties were investigated in simulated gastro and intestinal fluids under sink conditions. Results suggested that MCM-41 alone did not delay the release of melatonin significantly. Thus, the particles were coated with polyacrylic acid (PAA) to further slow the rate of release. Preliminary biological assays revealed that both uncoated and PAA-coated MCM-41 with melatonin did not significantly increase apoptosis nor ROS production compared to the control (no treatment) when added for 24 h to mouse microglial cells (BV2).

# Chapter 1 – Introduction

## 1.1 Mesoporous silica particles

### 1.1.1 Definition and discovery

Mesoporous silica particles (MSPs) are metal oxide materials with pores in the mesoscale dimension (2-50 nm). They were discovered from the study of crystalline zeolites. Zeolites are a family of microporous (< 2 nm) aluminosilicates prepared in 1756 and widely studied since then. In the first synthesis of zeolites aluminosilicate gels were used as precursors in strong alkaline conditions, using different mineral bases. After the introduction of organic amine molecules in the reaction mixtures, new structures were obtained. These organic molecules act as templates for the formation of the inorganic structure and when removed yield a porous material. Templating is a process during which a species forms a core structure around which material organizes and grows. The template imparts a structure directing effect on the material surrounding it. Nowadays, the term zeolite is used to indicate all microporous aluminosilica based solids with crystalline walls. Thus, zeolites include materials in which some silicon atoms have been substituted by another metallic element (e.g. Ge, Fe, Ti) [1].

MSPs were initially synthesised in order to expand the pore sizes of zeolites from the micropore to the mesopore range. This interest arose in response to the industrial need for more efficient porous materials which could be used in catalytic processes. The goal was to obtain porous materials that could crack high molecular weight hydrocarbons into lighter and valuable fuels and lubricants for the petrochemical industry [2]. Before the discovery of mesoporous materials in the early 90s, a patent describing the synthesis of similar materials was granted in 1971 [3]. However, the scientists involved did not identify the nature and potential of the mesoporous materials that they produced. Thus, the discovery of mesoporous silica is attributed to two other groups, which independently conceived different synthetic methods and published their work in the 1990s. These groups were the K. Kuroda team at Waseda University (Japan) and the Mobil Oil Corporation team (now ExxonMobil, USA) led by C.T. Kresge. Despite the fact that the Japanese group submission date was earlier than the filing date of the Mobil patent, the synthesis proposed by Kuroda et al. [4] is difficult to generalize, whereas the Mobil publications [5, 6] describe a more facile and versatile synthetic pathway. Mobil Oil Corporation materials were produced following the same concept of a structure directing agent or template used in the synthesis of zeolite. In mesoporous silica synthesis the template is generally a surfactant, which is an amphiphilic compound with both hydrophobic

and hydrophilic groups. The surfactant molecules self-assemble in order to reach a minimum free energy state and a reduction of surface tension, forming micelles. The driving force for this process is the increase of system entropy due to the loss of water around the hydrophobic region of the template molecules [7]. In the case of MSPs, the formation of micelles (micellization) is the first step of the synthetic process, followed by their aggregation. Surfactant head groups and silica are attracted to each other due to favourable electrostatic interactions. Subsequently silicates polymerize and condense surrounding the micelles, forming a silica network. In contrast to zeolites, the silica network in the wall of MSPs is not crystalline, but amorphous. After the removal of the templating agent, through solvent extraction and calcination, a porous structure is obtained. Surfactants are not the only compounds used for the synthesis of MSPs, in fact, other molecules can be successfully used to obtain mesostructures, e.g. folic acid [8]. In these cases the self-assembly of the template relies on supramolecular mechanisms.

### 1.1.2 Suitability for drug release applications

MSPs can be synthesised with a broad variety of pore structures and connectivity, e.g. 2-dimensional (2D) hexagonal and 3D-cubic. They possess high surface area (often > 700 $m^2/g$), large pore volume and narrow pore size distribution [9]. The key characteristics that make these materials suitable as drug delivery devices are their biocompatibility, ease of synthesis and design (e.g. pore and particle size tunability), ability to control the release of pharmaceutical compounds and their compatibility with different administration routes.

Active pharmaceutical ingredients with poor solubility and bioavailability, mild toxicity, high instability or unsatisfactory resistance to first-pass metabolism*[10], require innovative drug delivery solutions [11]. The first study of mesoporous silica materials in the field of drug release was performed by Vallet-Regi et al. [12] in 2001. Since then MSPs with different characteristics have been successfully employed as drug carriers [13, 14]. To tailor the release various strategies have been designed, including: modification of pore dimension and structure, functionalization of the internal pore space [15], external functionalization through PEGylation [16] or other polymers [17] and pore blocking systems [18]. Molecules inside the pores of mesoporous materials follow a random path. The first 60% of release was described by Higuchi as following a semi-empirical power-law expression [11]:

* First-pass metabolism = common way of referring to intestinal and hepatic metabolism. This process greatly decreases the concentration of the pharmaceutical active ingredient before it enters the systemic circulation.

$$Q=a+b\cdot t^{k} \quad \text{(Eq.1)}$$

This model can be applied to different carrier symmetries, e.g. planar, cylindrical and spherical. In this equation Q represents the amount of molecules released per unit exposed area of the carrier, t is the time and a, b and k are constants. This equation is related to the Weibull function which is used to describe release from both Euclidian and fractal systems. The constant a takes into account the initial delay and burst effects, while b is a kinetic constant. The exponent k is also known as the transport coefficient and it characterises the diffusion process. For ordinary case I diffusion in which the carrier does not swell (it is the case of mesoporous silica materials), k equals 0.5.

Amorphous colloidal non-porous silica particles are used as a food additive. It is approved by the European Union (additive E551) [19, 20]. The toxicity of colloidal silica has been thoroughly studied and is described in the Pharmacopeia[21]. However, the high surface area of MSPs, surface chemistry and tendency to interact with molecules in biological environments warranted their toxicological evaluation once again [11]. Clearly cell viability will vary depending on cell type, concentration or duration of exposure to the particles. In early studies no reduction in cells viability was noticed after the incubation of human primary antigen presenting macrophages with MSPs below 300 nm in particle size with a concentration of 100 µg/ml for 6 h or 24 h [22]. However, a small decrease in dendritic cells viability was observed after 24 h or 48 h of incubation with MSPs with particles sizes above 1 µm, at a concentration of 50 µg/ml [23]. Mesoporous silica toxicity has also been studied for various administrations routes. Kupferschmit et al. [24] demonstrated the high tolerability of these particles when administered orally to rats. In this study, doses up to 2000 mg/kg/day were administered and not toxic effects could be observed. A maximum tolerated dose (MTD) could not be reached. Fu et al. [25] tested the toxicity of MSPs administered through different exposure routes showing that MSPs are non-lethal when administered orally with a dose up to 5000 mg/kg, while the MTDs for intravenous, hypodermic and intramuscular administrations are 800, 1800 and 2400 mg/kg, respectively. Tamanoi et al. [26] determined that the maximum dose that could be intravenously injected to mice without any side effects was 100 mg/kg/day for a period of 10 days. Hudson et al. [27] studied *in vitro* and *in vivo* toxicity of three different types of mesoporous silica (MCM-41, SBA-15 and MCF) with different particle dimensions (150 nm, 800 nm and 4 µm) and pore sizes (3 nm, 7 nm and 16 nm). Three different cell lines were used for the *in vitro* studies: human mesothelial cells, mouse peritoneal macrophages and mouse myoblast differentiated into muscle cells. MSPs concentrations were varied between 0 and 0.5 mg/ml. For mesothelial and myoblast cells an increase in toxicity was measured with the increase in MSP concentration, while little or no toxicity was assessed for macrophages. For *in vivo* studies the

materials were injected subcutaneously (30 mg/ml) and at the sciatic nerve (50 mg/ml) in rats; and intraperitoneal (IP, 30 mg), subcutaneously (30 mg) and intravenously (IV, 6 mg) in mice. One rat died 3 days after the injection and another was suppressed because it developed difficulty moving its limbs, but all others (n = 40) did not exhibit any overt toxicity. In mice, after 24 h all IP injected with 30 mg of MSPs died or needed euthanasia and the MTD was subsequently determined to be 1 mg. Mice that received IV injections died within 15 minutes, while no toxicity was assessed for subcutaneously injected MSPs. It is important to note that in these studies very high administration doses were deliberately employed.

Another potential detrimental aspect of MSPs is related to their interaction with blood and, in particular, their haemolysis action and blood clot formation (thrombogenicity). Yildirim et al. [28] studied how bare MSPs and MSPs possessing different surface functional groups (ionic, polar, neutral, and hydrophobic) interact with blood cells. For the haemolysis assays red blood cells (0.2 ml) were incubated for 2 hours with MSPs (0.8 ml) with different concentrations (0.05-1 mg/ml) and the highest haemolytic activity was given by bare MSPs at concentration equal to 1 mg/ml. For the evaluation of thrombogenicity the cells were incubated for 5 minutes with the MSPs (concentrations = 0.1 – 1 mg/ml) and none of the MSPs presented significant thrombogenicity. Thus more toxicological evaluation of MSPs *in vitro* should be done for every different group of materials (nano- and microparticles, functionalized and naked, cylindrical pore structure and cage type, etc.) despite the large potential of these particles in the pharmaceutical and nanomedical applications [11]. Moreover, specific investigations are needed regarding other potential administration routes, such as nasal, ocular and pulmonary routes.

### 1.1.3 Synthetic mechanisms and silicate chemistry

According to the Kuroda group procedure [4], mesoporous silica particles called FSM-n (Folded Sheet Materials, where n stands for the number of C-atoms in the surfactant chain) can be synthetized by intercalation of kanemite, a sheet layered silicate, with a surfactant of the alkyltrimethylammonium type. The mechanism proposed relies on the deposition of the surfactant between the kanemite sheets, with subsequent silicate condensation forming the hexagonal array of pores. In the case of Mobil synthesis, MCM-n (Mobil Composition of Matter) particles can be obtained. Two different mechanisms for the formation of MCM-n were firstly assumed. The true liquid crystal templating (LCT) method and the cooperative mechanism. The LCT mechanism was firstly hypothesized in a publication by Attard et al. [29] and consists of two steps: (i) the formation

of the lyotropic liquid crystal phase by the surfactant, followed by (ii) the condensation of silicate species surrounding it. The liquid crystal structure is used as a template, around which the inorganic silica can polymerize and condense forming the framework of the mesostructure. This pathway is limited by the concentration of the surfactant, as ordered mesoporous materials should be formed only above the critical micelle concentration (CMC) of the particular surfactant used. In the cooperative mechanism [30], an organic-inorganic mesophase made of surfactant molecules and silicates is first formed. Subsequently silica oligomers polymerize and condense to form the amorphous silica walls. Davis et al. [31] suggested a new type of mechanism where the formation of an ordered liquid phase is not necessary for the formation of an ordered mesostructure since a concentration of surfactant below its CMC produced well-structured MSPs. According to Davis et al., the first step is the formation of a layer of silica on isolated rod-like micelles, followed by the aggregation of these in an ordered structure. The subsequent polymerization of silicate species leads to a hexagonal structure like material (Scheme 1).

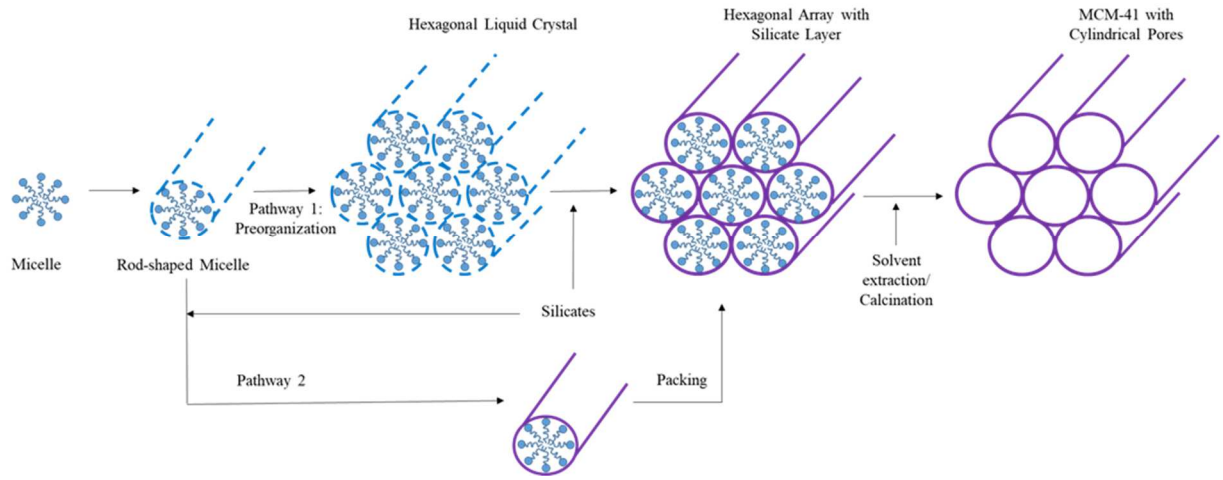


Scheme 1. Representation of the two possible synthetic pathways for the formation of MCM-41 materials (adapted from [32] and reprinted with permission from the publisher MDPI).

There are many silica precursors that are commonly used for the synthesis of mesoporous materials, such as sodium silicate ($Na_2SiO_3$), tetramethyl orthosilicate (TMOS) and tetraethyl orthosilicate (TEOS). When using sodium silicate, sodium chloride is formed under acidic conditions and removing it is time consuming and expensive. TMOS and TEOS have been used in many studies even if they require organic solvents, because of their poor water solubility, and extreme conditions of pH and high temperature [33]. The growth from solution of mesoporous silica is considered a sol-gel process in which there is a transformation of colloidal oligomeric particles dispersed in a liquid (sol) into a rigid non-fluid mass made up of a continuous network (gel).

Sol-gel processes involve inorganic alkoxide hydrolysis and condensation. Hydrolysis has the function to replace the alkoxide groups (-OR) of the silica source with hydroxyl groups (-OH), forming silanol groups (≡Si-OH). Whilst the condensation reaction implies the creation of siloxane bonds (≡Si-O-Si≡). This reaction can occur through the reaction of two silanol groups and the formation of a molecule of water as by-product or a silanol group and an alkoxysilane with an alcohol as by-product (Scheme 2).

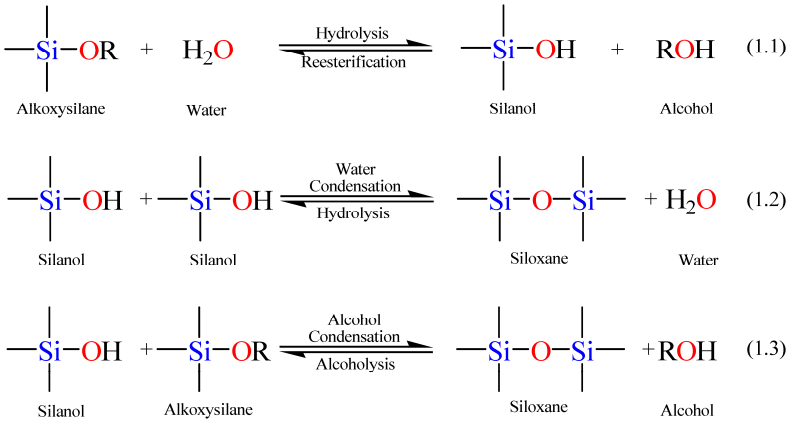


Scheme 2. a) Hydrolysis, b) water condensation, c) alcohol condensation. (Reprinted from [32] with permission from the publisher MDPI).

With the increase of siloxane bonds, the silica oligomers can aggregate into a sol, forming particles and then clusters. The gel is formed by the condensation of these clusters. The rates of both hydrolysis and condensation depend on the pH of the solution (Figure 1).

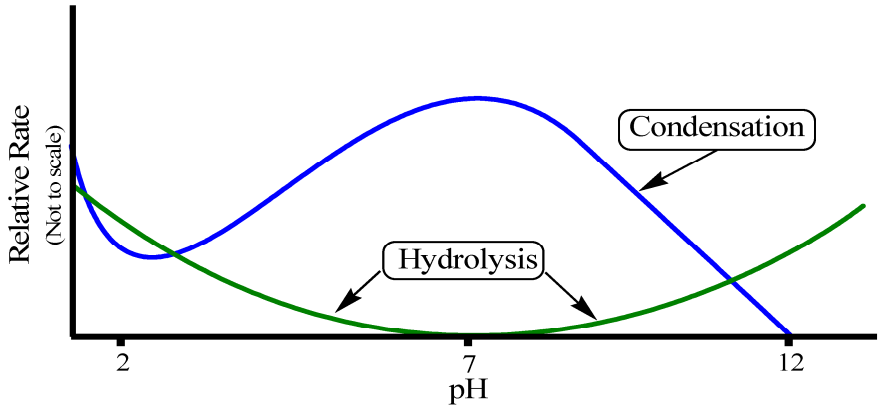


Figure 1. The inverse relationship between hydrolysis and condensation rates (reprinted from [32] with permission from the publisher MDPI).

The mechanisms of the two reactions are affected by the presence of an acid or base catalyst. In acidic conditions (Scheme 3) the first step of the hydrolysis is represented by the electrophilic attack of the proton on an alkoxide oxygen atom. The second step is an SN2 nucleophilic substitution, where a water oxygen attacks the silicon from the backside. A transition state is formed and then an alcohol molecule and a proton are released, forming a silanol group. The second step is the rate-determining step (RDS). The condensation reaction with an acid catalyst starts with the electrophilic attack of the proton on the oxygen of the hydroxyl group of the silanol. The protonated silanol group reacts with an un-protonated one, forming a siloxane bridge and releasing a hydronium cation.

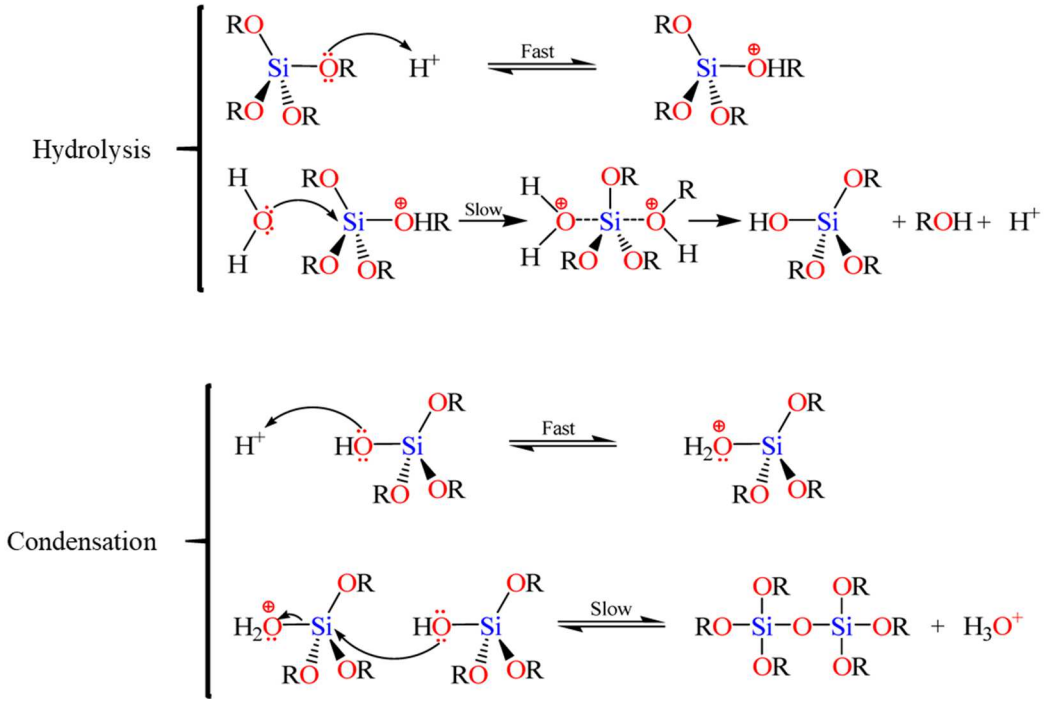


Scheme 3. Hydrolysis and condensation steps under acidic conditions (modified from [32] with permission from MDPI).

In the base catalysed reaction (Scheme 4) the hydrolysis begins when a hydroxide ion attacks an alkoxide silicon atom. This step is a SN2 nucleophilic substitution which leads to the formation of a silanol and an alkoxide ion. The condensation reactions involve the abstraction of a silanol proton by the hydroxide ion, forming a siloxide ion, followed by the reaction between the latter and the silanol. The second step is a SN2 substitution in which a siloxane bond is formed and it represents the RDS on the condensation steps [32].

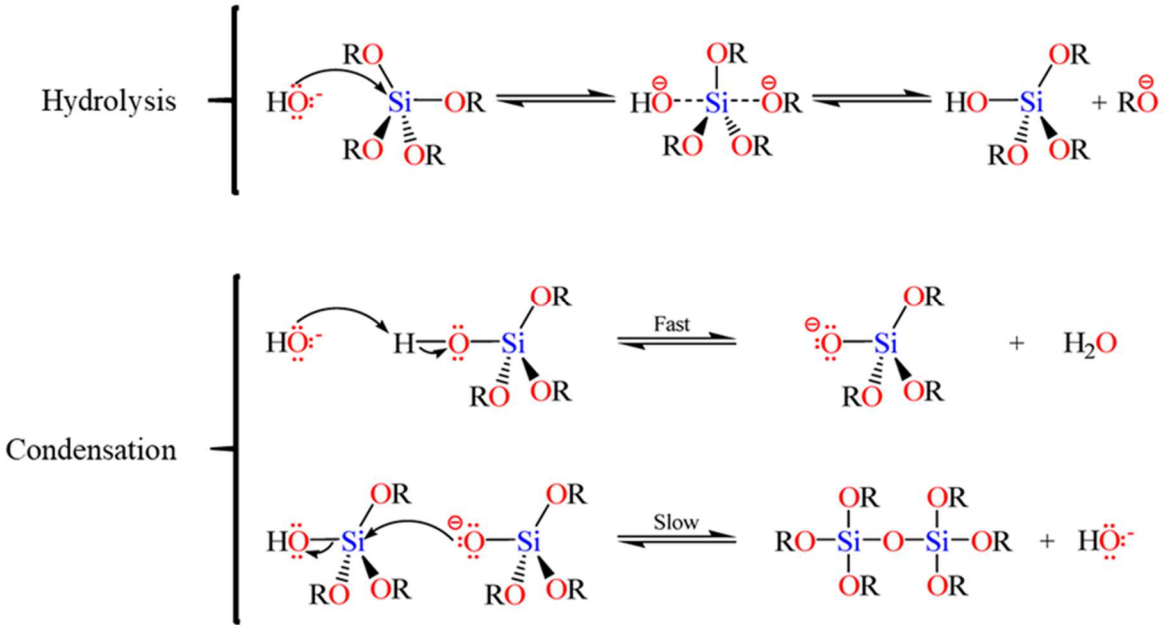


Scheme 4. Hydrolysis and condensation mechanism under basic conditions (modified from [32] with permission from MDPI).

## 1.1.4 Different templating agents

### 1.1.4.1 Surfactants

Surfactants are amphiphilic molecules typically made up of a hydrophobic tail and a hydrophilic head. They are classified according to their head group charge into anionic (negatively charged), cationic (positively charged), non-ionic (neutral) and zwitterionic (amphoteric, they contain both acidic and basic groups). More exotic types of surfactants used to prepare MSPs are the gemini, which possess two hydrophobic chains and two cationic head groups; and the bolaform type, which have one hydrocarbon chain and two charged groups. Some block copolymers, e.g. triblock co-polymer with poly(ethylene oxide PEO)-b-poly(propylene oxide PPO)-b-poly(ethylene oxide PEO), can also be used as surfactants for the synthesis of mesoporous materials thanks to their hydrophobic and hydrophilic blocks in their structure which enable micellization. They are relatively cheap, biodegradable and allow to synthesise materials with large pore sizes [34].

The interactions between the surfactant and the inorganic precursor molecules determine the formation of a mesophase and so the final mesostructure. These interactions depend on the charge on the head groups of the surfactant, $S^+$ or $S^-$, on the inorganic silica species, $I^+$ or $I^-$, and on the presence of mediating ions, i.e. $X^-$ or $M^+$. All combinations that allow Coulombic attractions between the surfactant and the inorganic species are favourable for the mesophase formation. The simplest case, considered to be the direct pathway, is represented by the situation in which S and I

have opposite charges in the synthesis conditions (i.e. at the solution pH). Indirect pathways are cases in which S and I have the same charge and a mediating ion is necessary to induce the interaction. Other ionic interactions are possible. In fact, neutral ($S^0$) or non-ionic ($N^0$) species can interact with uncharged inorganic precursor molecules ($I^0$) through hydrogen-bonding or covalent bonding between the surfactant and the inorganic species (S-I) can occur (Figure 2).

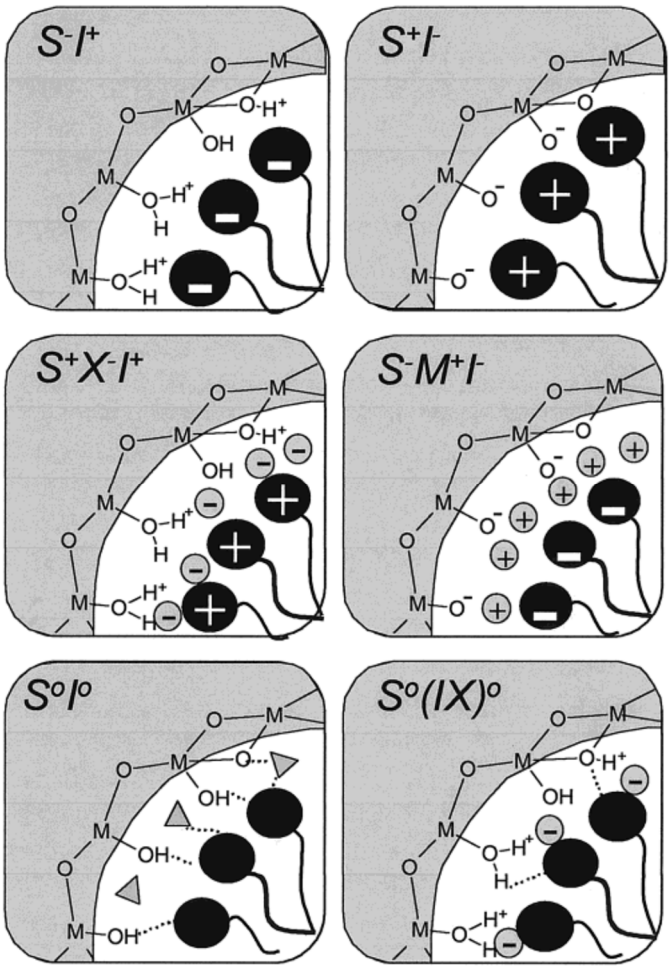


Figure 2. Different interactions between surfactant (S) and the silica species (I). $M^+$ and $X^-$ are the mediating ions. The triangles represent the solvent molecules, while the dashed lines correspond to hydrogen bonds (reprinted from [1] with permission of ACS).

### 1.1.4.2 Non-surfactant macromolecules

Ordered MSPs can also be synthesised using non-surfactant molecules as pore forming agents. As reported by Atluri et al. [8], folic acid is an efficient template for the production of mesoporous silica materials with hexagonal pore structure. Through this synthesis NFM-1 (Nanoporous Folic Acid Materials) particles are formed. In this case, no micelles are formed, but the mesophase formation relies on the self-organization of the pterin groups of folic acid (Figure 3). The self-

assembly of folic acid is due to the Hoogsteen-type hydrogen bonding in between the amino groups and, in particular, between the electronegative nitrogen and oxygen and the hydrogens atoms [35]. The hydrogen bond formation is the driving force for the assemble of pterin rings into tetrameric rings with the glutamate groups at the exterior part of the pterin rings. The silane 3-aminopropyl triethoxysilane (APTES) is used as a CSDA to obtain the desired constructive interactions between silicate oligomers and the glutamic groups of folic acid, which are both negatively charged at the synthetic conditions (pH).

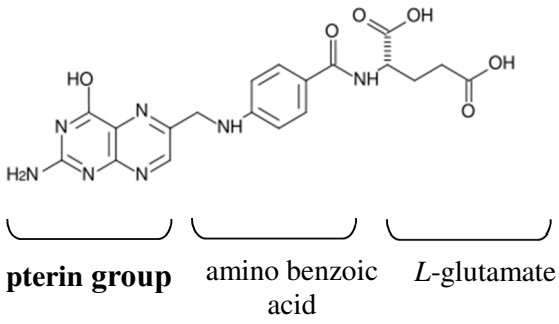


Figure 3. Molecular structure of folic acid.

## 1.1.5 Different pore structures

MSPs with different cylindrical or cage-type mesostructures can be synthesised, for example lamellar, 2D-hexagonal, 3D-hexagonal, 3D-cubic and including bicontinuous cubic (Figure 4b).

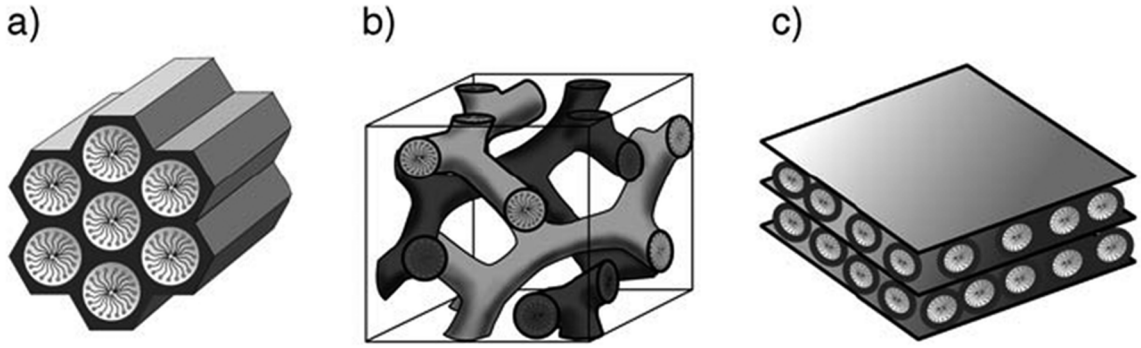


Figure 4. Schematic models for different types of pore structure: a) hexagonal, b) cubic and c) lamellar [36].

The variation of one or more synthetic parameters can lead to a change in the interactions between the template and the silica species. Thus, tuning of the mesopores can be done through the modification of the synthetic conditions, e.g. temperature, pH or addition of co-solvents. The packing parameter (g) of the surfactant is one of the key factors for the determination of the mesostructure [37] and may be calculated from Eq.2:

$$g=V/(a\cdot l) \qquad \text{(Eq. 2)}$$

where V stands for the total volume of the surfactant hydrophobic chains, a is the area of the hydrophilic head group, while l represents the length of the surfactant tail. To different values of the packing parameter correspond different micelles shapes and, thus, different mesostructures. An increase of g means a decrease in the micelles-silicates interface curvature. Spherical micelles form when g is lower than 1/3, rod-like micelles are observed when g is between 1/3 and 1/2, while lamellar micelles are present if the value of g is equal to 1. When the packing parameter is higher than 1 reversed micelles form in the solution (Figure 5).

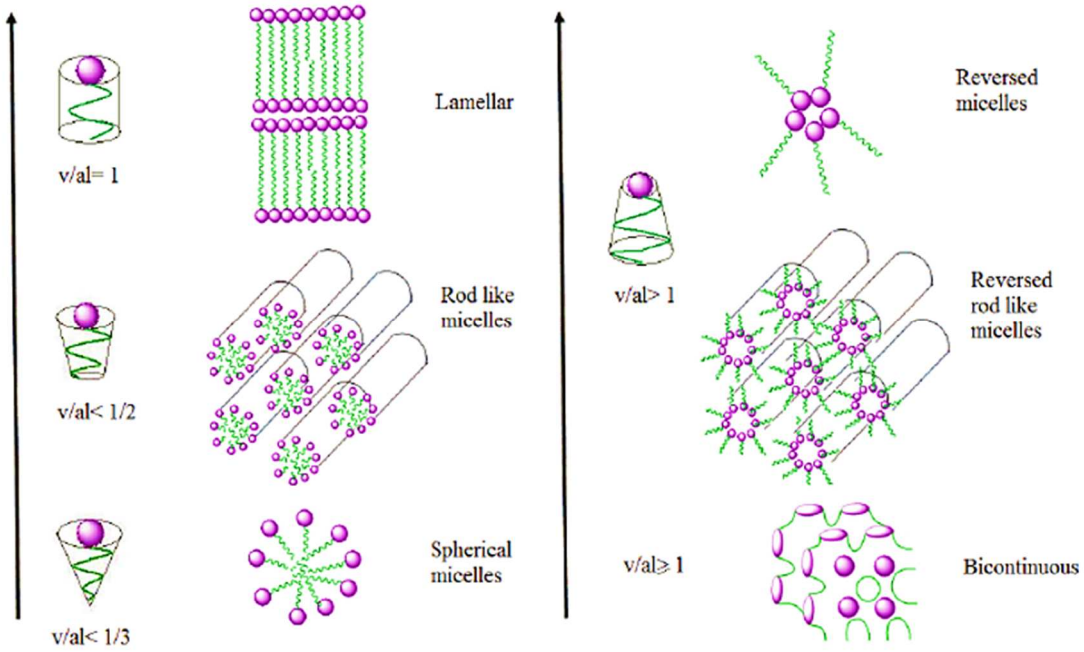


Figure 5. Correlation between packing parameter values and micelles shape (reprinted from [38]).

## 1.2 Melatonin

Melatonin (N-acetyl-5-methoxy tryptamine) is a hormone produced by the pineal gland, a small endocrine gland, located in the centre of the human brain [39]. The secretion of melatonin occurs mostly during the night and light suppresses its release (Figure 6). Melatonin release is regulated by the so-called master circadian clock, located in mammals in the suprachiasmatic nuclei (SCN) in the hypothalamus [40]. The precursor of melatonin is the amino acid tryptophan, which is hydroxylated to serotonin. The latter is then acetylated to form N-acetylserotonin and this is finally converted into melatonin through methylation (Scheme 5).

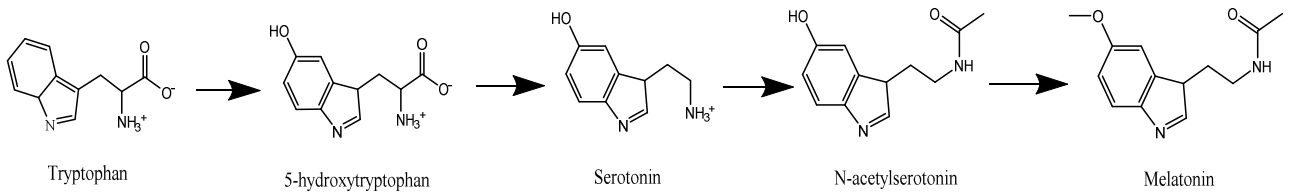


Scheme 5. Sequence of reactions from tryptophan to melatonin.

Melatonin feeds back information on the timing of external day and night to the SCN, rich in melatonin receptors, modulating circadian rhythms [40]. Circadian rhythms are endogenously generated cycles of about 24 hours that occur in many biological and behavioural processes, including sleep/wake cycle, hormones release, metabolism. Circadian clocks are located in each of our cells, they are called peripheral clocks. They are synchronized by the master clock which is the only clock capable to synchronize to the light-dark cycles through information directly received by the retinas [41]. Other *Zeitgebers* (time givers in German) such as food [42] or temperature can also synchronize both the master and peripheral clocks. The sleep/wake cycle is thought to be affected by both endogenous and exogenous melatonin [43], [44]. The melatonin receptors are two G-protein coupled receptors, known as MT1 and MT2.

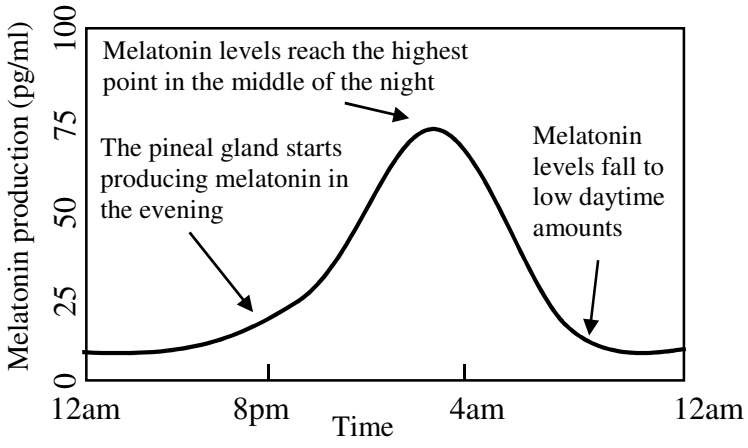


Figure 6. Representative daily melatonin oscillatory pattern.

In humans these receptors have different molecular structures and pharmacological characteristics. It is hypothesised that they might have different functions, but determining these functions and studying the receptors is arduous, as their densities in tissue are very low [45].

### 1.2.1 Clinical Uses

Exogenous melatonin is mostly used in the treatment of circadian disorders [46, 47], delayed sleep phase syndrome or shift-work, but other potential actions of this hormone on the human organism have been hypothesised, for example it may be capable of regulating some aspects of the immune system [48]. In currently available melatonin formulations most of the active ingredient undergoes first-pass metabolism breakdown, which leads to low bioavailability of the hormone [49]. Thus new melatonin formulations are needed to meet the demands of particular groups of people, such as elderly with circadian rhythms dysregulations [50], shift workers [51] and frequent travellers with jet lag [52]. Other target population with sleep/wake disorders that require special formulations are those affected by neurocognitive disorders, including schizophrenia, bipolar disorder or dementia [45]. Sleep and circadian rhythm disruption are also strictly related to depressive disorders, but current antidepressants do not treat them. Thus formulations that can target MT1 and MT2 receptors might play a key role in the treatment of the regulation of sleep-wake cycles in depression patients, which might contribute to their depressive disorder too [45].

### 1.2.2 Available formulations and administration routes

Melatonin has a short plasma half-life ($t_{1/2}$ < 30 minutes) and variable bioavailability due to high first-pass metabolism [53]. Different formulations have been studied in order to improve melatonin concentration in the bloodstream and, therefore, its efficacy:

i. *sublingual/transbuccal delivery*: in this case the absorbed active ingredient reaches the bloodstream directly, through the blood vessels present in the mouth, avoiding the first-pass metabolism. Among the disadvantages of this administration route there is the impossibility of accommodate large doses of drug and the low adsorption area [54]. Dawson et al. [55] studied the efficacy of transbuccal melatonin formulations for the treatment of insomnia in elderly people, finding no significant clinical benefit on any polysomnographic (PSG) measure of sleep quality;
ii. *transdermal delivery*: Kanikkannan et al. [56] demonstrated the feasibility of patches for the transdermal release of melatonin through rat skin, while Dubey et al. [57] used ethanolic liposomes to deliver the hormone efficiently. This type of administration allows to skip hepatic clearance, but the difficulties reside in overstepping the stratum corneum (the thick protecting outer layer of the skin layer) [57]. Despite this drawback, Aeschbach et al. [58] reported that transdermal melatonin delivery increased plasma melatonin levels with a peak

concentration after 8.58 h. This formulation increased sleep efficiency, total sleep time and decrease wakefulness after sleep onset but only in the last one-third of sleep time;

iii. *intravenous injections*: Mallo et al. [53] demonstrated the suitability of this administration route. In their study it brings melatonin up to nocturnal levels after 1-2 hours. Intravenous administration allows the active ingredient to reach the bloodstream directly, but its main disadvantage is feasibility;

iv. *intranasal administration*: the main advantage of these types of formulation is the ease of use, while the drawback is the short residence time, which leads to low bioavailability of the active ingredient. Mao et al. [59] developed an intranasal melatonin formulation using microspheres made of starch. It presented long deposition time in the nose, but a hormone entrapment ratio of about 11%;

v. *oral administration*: this is one of the easiest and most convenient administration routes for all target groups, the main disadvantage is the clearance of a significant amount of active ingredient through first-pass metabolism. To maintain a melatonin concentration in the bloodstream above the effective range of concentrations, it is necessary to provide high doses or recurring low doses during the night [49, 60]. Among oral formulations, Circadin (registered trademark of Neurim Pharmaceutical) appears to be one of the most effective for the short-term treatment of primary insomnia for people over 55. This formulation contains 2 mg of melatonin and its prolonged release (PR) of melatonin lasts between 6 and 8 hours and its use was officially approved by the European Medicines Agency (EMA) in 2007 (for details see http://www.ema.europa.eu/ema). Circadin was approved by the Therapeutic Goods Administration, a division of the Australian Government Department of Health and Ageing, in 2009, following recommendations by the Australian Drug Evaluation Committee (ADEC) [61]. This PR formulation has been designed to be effective for a particular sleep disorder occurring in a precise population, so many other sleep disorders and group pf people still require personalized formulations.

## 1.3 Aims of this thesis

The goal of this project was to use mesoporous silica particles to control the release of melatonin, in order to obtain an innovative formulation with a release profile different from those currently available commercially.

This research focused on the synthesis and characterisation of MSPs for the delayed release of melatonin. To change the release profile of melatonin, the hormone was loaded into MSPs and the pores were capped using a pH-sensitive polymer, named polyacrylic acid (PAA). The materials were characterised using X-Rays diffraction (XRD), scanning electron microscopy (SEM), transmission electron microscopy (TEM), nitrogen adsorption isotherm, thermogravimetric analysis (TGA), dynamic light scattering (DLS) and Fourier-Transformed infrared rays (FT-IR). The release of the melatonin from these formulations was tested in simulated gastric fluid (SGF, pH 1.2) and simulated intestinal fluid (SIF, pH 6.8) through a dissolution apparatus under sink conditions. Subsequently, the effects of loaded MSPs on murine BV2 cells were determined *in vitro*. Specifically, apoptosis and cytotoxicity in terms of reactive oxygen species (ROS) production were investigated.

The specific aims of this project were:

- load melatonin into mesoporous silica particles;
- coat the melatonin loaded particles with polyacrylic acid;
- characterise the uncoated and PAA-coated particles;
- test and understand the release from uncoated and PAA-coated mesoporous silica materials;
- compare the release of melatonin from uncoated and PAA-coated materials with the dissolution of free melatonin and the release of the hormone from a currently available formulation (Circadin);
- test the formulation *in vitro* on a brain cell line and perform a preliminary cytotoxicity assessment.

# Chapter 2 – Materials and Methods

## 2.1 Chemicals

All chemicals were purchased from Sigma Aldrich and used as received without further purification, unless otherwise specified. Biological assays kits were purchased from Merck Millipore.

## 2.2 MCM-41 synthesis

2.5 g of *n*-hexadecyltrimethylammonium bromide ($C_{16}$TMABr) were dispersed in 50 g of distilled water, 13.5 g of aqueous ammonia ($NH_{3aq}$) and 60 g of ethanol (EtOH). The mixture was stirred for 2 hours at room temperature (200 rpm). The pH was measured (the value was 12.460) and then 4.7 g of tetraethyl orthosilicate (TEOS) were added quickly under stirring (300 rpm). The final molar ratio in the synthesis was: CTAB: $H_2O$: $NH_3$: TEOS: 0.3: 123: 34.6: 57.7: 1. The resulting mixture was stirred for 2 hours at room temperature (300 rpm) and pH value was checked again (the value was 11.236). The bottles were left in the oven at 100°C for 24 hours and then the pH was measured for the last time (the value was 9.447). The solvent was removed through filtration and then the surfactant was partially removed through extraction with a mixture of EtOH and hydrochloric acid (HCl) (8:2 v/v) for 2 hours at 80°C (300 rpm). The sample was recovered through filtration and dried at room temperature for 12 hours and then calcined at 550°C for 3 hours.

## 2.3 MCM-41 loading with 10, 20 and 30wt% melatonin

1375 mg of MCM-41 were dispersed into 250 ml of EtOH and sonicated for 30 minutes. 137.5 mg (10wt%), 275 mg (20wt%) or 412.5 mg (30wt%) of melatonin were dispersed in EtOH (concentration = 5 mg/ml) and stirred at room temperature for 30 minutes (300 rpm). The melatonin solution was poured into MCM-41 solution and stirred at room temperature for 30 minutes (300 rpm). The solvent was removed via controlled evaporation with a rotary evaporator (stirring rate 100 rpm, bath temperature 40°C) connected to a programmable vacuum pump. The pressure was progressively decreased using the following program: 800 mbar for 10 minutes, 100 mbar for 20 minutes and 1 mbar for half an hour. The final powdered product was stored at room temperature in a vacuum desiccator.

## 2.4 Coating of MCM-41 with Polyacrylic acid (1:2 wt ratio)

200 mg of MCM-41 loaded with a theoretical 20wt% of melatonin was dispersed into 140 ml of tetrahydrofuran (THF) by stirring for 20 minutes at room temperature (300 rpm). 400 mg of polyacrylic acid (PAA) were dissolved into 100 ml of THF and stirred for 20 minutes at room temperature (300 rpm). PAA solution was mixed with MCM-41 solution and the mixture was stirred for 30 minutes at room temperature (300 rpm). The solvent was evaporated via controlled evaporation with a rotary evaporator connected to a programmable vacuum pump. The pressure was controlled through the same program used to load melatonin into the materials. The final powdered product was stored at room temperature in a vacuum desiccator.

## 2.5 Melatonin in PAA

150 mg of PAA were dissolved into 50 ml of EtOH and 14.2 mg of melatonin were dissolved in 2.88 ml of EtOH by stirring at room temperature for 20 minutes (300 rpm). Melatonin solution was added to the PAA one and the mixture was stirred for 20 minutes at room temperature (300 rpm). The weight ratio between PAA and melatonin was the same as in the sample of PAA-coated MCM-41 with melatonin. EtOH was removed via controlled evaporation with a rotary evaporator connected to a programmable vacuum pump, using the same pressure control program used for PAA-coated MCM-41 with melatonin. The final powdered product was stored at room temperature in a vacuum desiccator.

## 2.6 Release Measurements

The release profiles of melatonin from uncoated and PAA-coated MCM-41 were measured in simulated gastro (SGF, pH 1.2) and intestinal fluids (SIF, pH 6.8) under sink conditions. In order to obtain the release profiles a dissolution apparatus coupled to a UV-Vis spectrometer via a peristaltic pump was utilized. These release profiles were then compared to the dissolution curve of commercially available melatonin in the same media. Moreover, a prolonged release commercially available product, known as Circadin, was tested in the same conditions and used as a reference.

The instrument used for these measurements was an Agilent Technologies 708-DS Dissolution Apparatus with a Cary 60 UV-Vis spectrophotometer. The software used to analyse the data was UV Dissolution by Agilent. The temperature of the dissolution bath was maintained constant at 37°C to mimic the body temperature and the stirring rate was 50 rpm during all sampling time. The standard (melatonin) was dropped into the standard vessel as free powder, Circadin was dropped as

received (pill) or completely crushed. The uncoated and PAA-coated MCM-41samples loaded with melatonin were dropped using a cellulose capsule with a fast disintegration rate (< 2 minutes) as containers.

## 2.7 Biological Assays

Two biological assays were performed in order to obtain preliminary data on the effects on apoptosis and oxidative stress of both uncoated and PAA-coated melatonin-loaded MCM-41. The apoptosis assay was useful to determine if the formulations were cytotoxic, while the oxidative stress assay gave information about the cell's wellbeing. The cells used in these studies were BV2 cells. This is a brain microglial cell line from mice C57BL/6. In both cases cells were incubated with the MSPs formulations for 24 hours.

To test the reaction of cells to the new formulation different suspensions were prepared containing: MCM-41 without melatonin, melatonin loaded MCM-41, PAA-coated MCM-41 with melatonin or free melatonin at different concentrations.

To perform these assays, cells were treated with the following procedure:

- Culture BV2 cells in a flask;
- Passage cells;
- Prepare well plates:
    a) In each well: 0.2 mL of media with cells and 2 mL of fresh media;
    b) Leave the plate in the cell culture incubator for 48 h hours.
- Add 100 µL of MSPs suspension in each well;
- Add 1 µL of melatonin solution in each well;
- Add 1 µL of lipopolysaccharides (LPS, concentration = 1 µg/mL) as a positive control;
- Incubate for 24 hours.

The final concentration of the MSPs in each well was 50 or 100 µg/ml. The final concentration of melatonin in each well was 9.65 or 19.3 µg/ml.

Each sample was analysed in triplicates. The average value and standard deviation were calculated for each set of data. A statistical test (T-test) was used to determine if the data obtained were significantly different from the negative control.

### 2.7.1 Apoptosis

Apoptosis, i.e. programmed cell death, assays can give information about the viability of cells when they are exposed to new conditions (e.g. presence of particles). Cells respond to external stimuli by activating intracellular processes which result in characteristic changes of the cells. For example, when undergoing apoptosis, cells can react by externalizing phosphatidylserine (PS) on their surface, degrading specific cellular proteins or losing membrane integrity [62].

The Muse Annexin V and Dead Cell Assay was used. Annexin V is a calcium-dependent phospholipid-binding protein which possesses high affinity for PS [63] and thus helps detecting the early and late apoptotic stages of cells. Moreover, a dead cell marker was used to determine the cell membrane integrity. Hence, it was possible to distinguish four different cells populations: live, early apoptotic, late apoptotic and dead cells.

The protocol for this assay is the following:

1. Detach cells from wells: remove media, wash with phosphate-buffered saline (PBS), add 0.2 ml Trypsin in each well, incubate for 5-10 minutes;
2. Collect cells in 15 ml tubes, add 1 ml of media with 1% FBS in each tube;
3. Centrifuge (200 rpm for 3 minutes), remove supernatant and resuspend cells in 1 ml PBS;
4. Work on ice: add 100 µl of Muse Annexin V and Dead Cell Reagent and 100 µl of cells in suspension in each 2 ml tube;
5. Incubate for 20 minutes at room temperature in the dark;
6. Cut the tubes caps;
7. Analyse with the Muse Analyser.

### 2.7.2 Reactive Oxygen Species (ROS) production

The term ROS indicates the formation of chemically reactive radicals and non-radical molecules derived from molecular oxygen (e.g. superoxide, singlet oxide and peroxide). It is known to play a role in different cells functions, such as signalling and regulation, activation of apoptosis or necrosis [64-66].

The Muse Oxidative Stress Kit was used to identify the percentage of cells undergoing oxidative stress by detection of intracellular superoxide radicals. The reagent present in the kit contains dihydroethidium (DHE) which has been largely utilized to assess the presence of ROS in cellular populations. DHE permeates into cells and upon reaction with superoxide ions it undergoes

oxidation. The product of this oxidation is a DNA-binding fluorophore ethidium bromide which produces red fluorescence. Thanks to this assay it is possible to identify two different cells populations: ROS negative and ROS positive cells.

Protocol:

1. Work on ice: use the remaining cells from Apoptosis Assay point 3, but instead of adding PBS, add 1 ml of Buffer from ROS Kit in each tube and redisperse cells;
2. Prepare intermediate solution as follows: dilute muse oxidative stress reagent 1:100 (e.g. for 20 samples: add 2 µl of use Oxidative Stress Reagent stock solution to 198 µl of 1X Assay Buffer);
3. Prepare working solution as follows: dilute Muse Oxidative Stress Reagent intermediate solution 1:80 in 1X Assay Buffer (e.g. for 20 samples: 47.5 µl of intermediate solution in 3752.5 µl of 1X Assay Buffer);
4. Add 190 µl of Muse Oxidative Stress working solution to 100 µl of cells;
5. Leave in the incubator at 37°C for 30 minutes;
6. Cut the tubes caps;
7. Analyse with Muse Analyser.

## 2.8 Characterization Techniques

### 2.8.1 X-Ray Diffraction (XRD)

In order to confirm the mesoporous structure of the materials and to determine the physical state of melatonin after its loading into the pores XRD was used.

This analysis technique uses electromagnetic waves to determine the atomic and molecular structure of a sample. The basic principle behind it is the Bragg law (Eq. 3), which describes the diffraction and constructive interference of X-rays when reflected by the atomic planes of the sample.

$$2dsin\theta = n\lambda \qquad \text{(Eq.3)}$$

where $d$ is the interplanar spacing $d_{hkl}$ (hkl: Miller indices). Note that just hk indices can be used as indices in the case of 2D materials such as MCM-41. The Bragg angle is $\theta$ ($2\theta$ is the angle between incident and reflected beam), $n$ is the order of the interference (normally $n = 1$) and $\lambda$ is the wavelength.

Mesoporous silica diffraction peaks give information about the order and pore structure (e.g. cubic, hexagonal, etc.) of the particles. There are no sharp peaks representing the crystal structure as MSPs

have amorphous walls. A typical MCM-41 plot includes three or four peaks in the low-angle 2θ region (below 2θ = 6°): the first and strongest in intensity is the (10) reflection occurring around 2°, the second (11) and third (20) between 3.5° and 5° and the last one (21) just below 6° (Figure 7a). It is quite rare to obtain more than four peaks and often only the first three are observable. Using the peak spacing it is possible to estimate the unit cell value, i.e. $a$, through the following equation :

$$a = \left(\frac{2}{\sqrt{3}}\right) d_{10} \qquad \text{(Eq. 4)}$$

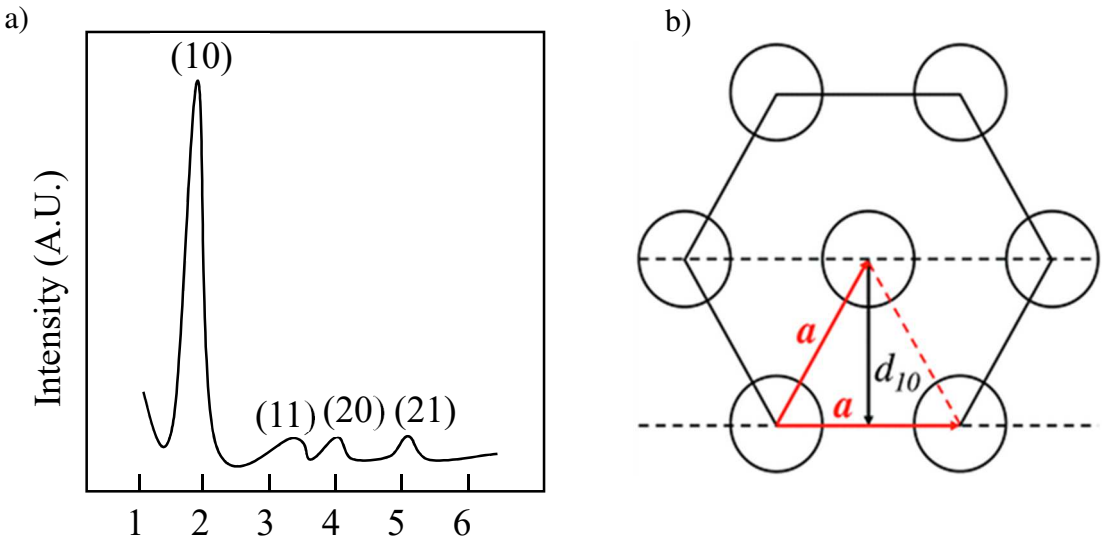


Figure 7. a) Characteristic XRD curve of MCM-41; b) MCM-41 pore arrangement and characteristics parameters: unit cell ($a$) and the lattice plane spacing $d_{10}$ which corresponds to the Bragg peak with indices (10) (reprinted from [67] with permission of RCS).

The XRD curve for crystalline melatonin, instead, is characterised by sharp peaks between 10° and 60° 2θ. The peak pattern is asymmetric and the more intense peaks can be found between 10° and 30° 2θ [68].

All the XRD analysis were performed using a Bruker D8 Discover diffractometer equipped with Cu-Kα radiation as X-Ray source (λ = 1.5406Å) and the data were collected and analysed with DIFFRAC.SUITE™ software.

### 2.8.2 Scanning Electron Microscopy (SEM)

SEM analysis was used to confirm the MSPs morphology and size, as well as to visually identify the presence of the polymeric coating.

In a SEM an emitter, often a tungsten filament or single crystal, generates an electron beam which interacts with the surface of the sample. The beam scans the surface of the sample without passing through it. Different types of signals emerge from the sample (secondary electrons, backscattered electrons, X-rays, etc.) and they are captured by the detectors to produce an image of the sample topography. Conventional SEM works under high vacuum, as gas at atmospheric pressure can attenuate the electron beam, but other types of SEM modes allow to work at low vacuum or in wet conditions. With this technique it is possible to observe particles in the range of nano to micrometer size.

Scanning electron microscopy images were captured with JEOL 7100F Field Emission Scanning Electron Microscope with a hot (Schottky) electron gun (1.2 nm resolution). Samples were prepared without gold coatings and imaged at magnifications between x1000-x30000, at 1.5kv using Gentle Beam mode.

### 2.8.3 Transmission Electron Microscopy (TEM)

TEM imaging was used to observe the pore structure of the synthesised materials.

In this technique the beam of electrons generated by the electron gun is transmitted through the specimen. After the source, often a tungsten filament, produces the beam, the lenses of the TEM focus the electrons to the desired location. It is possible to manipulate the beam using a magnetic or an electrostatic field. As in the case of SEM, TEM operates under vacuum. Transmitted and scattered electrons from the sample give information about its structural properties. In the resulting image, the dark contrast represents high electron density areas which have a greater interaction with the electron beam. On the other hand, light contrast corresponds to areas of less electron density. In the case of mesoporous materials, the light contrast can be identified with the pores.

TEM images were obtained with a JEOL-3000F microscope, operating at 300 kV (spherical aberration: 0.6 mm; resolution 1.7 Å). Images were collected between x40,000-80,000 magnification.

## 2.8.4 Nitrogen Adsorption Isotherm

This technique allowed to determine the textural properties of materials. In the case of MSPs it is convenient for the measurement of surface area, pore volume and pore size. The adsorption isotherm is a quantitative analysis where the amount of gas adsorbed onto a surface at a fixed temperature is plotted as a function of pressure.

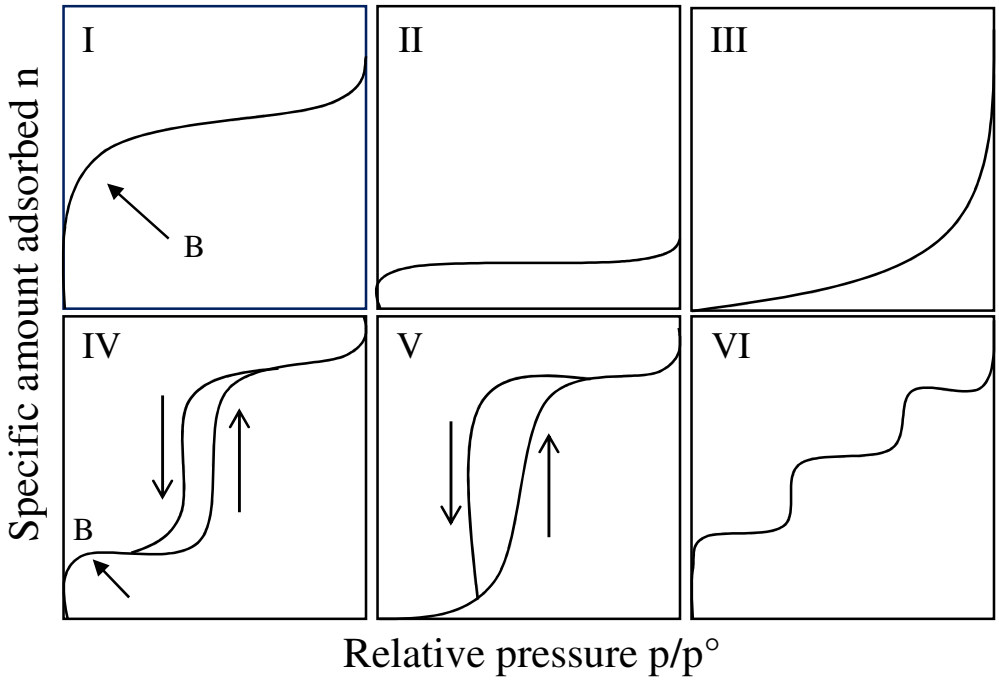


Figure 8. Types of adsorption isotherm curves: I) microporous solids, II) non-porous or macroporous adsorbent (point B: indicates monolayer coverage), III) few systems, e.g. nitrogen on polyethylene, IV) mesoporous materials, V) porous adsorbents in which adsorbent-adsorbate interaction is weak, VI) multilayer adsorption on a non-porous surface.

The mechanism of adsorption starts with the formation of a monolayer of nitrogen adsorbed onto the surface. This is followed by multilayer formation and, if pores are present, by capillary condensation. The adsorption takes place at a temperature below the critical point of the adsorbate (in this case, nitrogen), as under this temperature the amount of gas adsorbed on the material increases with pressure increase. According to the IUPAC recommendation there are six different types of adsorption isotherm plots [68] (Figure 8). The type IV is the isotherm curve associated with mesoporous materials and it consists of two curves: adsorption and desorption of nitrogen molecules from the materials surface and pores. The pore filling with nitrogen occurs by capillary condensation and, if it takes place above a relative pressure, a hysteresis is present in the desorption curve.

There are different mathematical models which are useful to describe the adsorption and desorption phenomena. All the surface data presented in this thesis were determined using BET (Brunauer–Emmett–Teller) model for multilayer adsorption of nitrogen molecules. Multilayer models are an extension of Langmuir's monolayer model and are based on three hypotheses:

1) gas molecules are physically adsorbed onto the materials surface, forming different layers;
2) no interaction is present between each adsorption layer;
3) Langmuir's approach can be applied to each layer.

The BET equation is the following:

$$\frac{P}{V(P_0 - P)} = \frac{1}{cV_m} + \frac{(c-1)P}{cV_m P_0} \qquad \text{(Eq. 5)}$$

where P and $P_0$ are the equilibrium and saturation pressure of the adsorbate at the temperature of adsorption, V is the adsorbed gas quantity, $V_m$ is the monolayer adsorbed gas quantity and c is the BET constant.

The BJH (Barrett-Joyner-Halenda) is a method often used for the calculations of the pore size distribution (PSD) and it is based on the Kelvin equation:

$$\ln \frac{P}{P_0} = -\frac{2\nu\gamma}{r_K RT} \qquad \text{(Eq. 6)}$$

where $r_k$ is the mean radius curvature of meniscus, ɣ is the surface tension and υ is the molar volume of the adsorptive. The temperature is 77.53 K and R is the gas constant. It has been proven that the BJH method underestimates the pore size of the materials even when the pores are around 20 nm [69].

The density functional theory (DFT) method of calculating PSD, is considered to give a more reliable description of the adsorption phenomena and a more accurate value of the PSD. The DFT approach is based on the physical adsorption of non-specific gases and can be described using Lennard-Jones intermolecular potentials for both fluid-fluid and solid-fluid interactions [70]. The PSD plots presented in this thesis are based on the DFT method with the cylindrical pores model.

Nitrogen adsorption isotherm measurements were performed with a Micromeritics TriStar II Surface Area and Porosity instrument and the data were analysed with TriStar II 3020 software.

Prior to the adsorption isotherm analysis, the sample must undergo a process called degassing. This step removes any adsorbed gas or vapour (e.g. water) which could alter the gas adsorption measurements. Degassing involves heating the sample in a tube under vacuum and then backfilling the tube with nitrogen. In this project a Micromeritics VacPrep 061 Sample Degas System was used and every sample was heated at 60°C overnight.

### 2.8.5 Thermogravimetric analysis (TGA)

This technique was used to determine the amount of melatonin loaded within the MSPs pores and the amount of PAA present inside them.

This analysis method is based on the measurement of the sample weight loss with the temperature increase in an oxygen containing atmosphere, so that decomposition can occur.

TGA was performed on TGA 2050 Thermogravimetric Analyser by TA Instrument. The data were collected and analysed with Advantage Software. The mass of the samples analysed varied between 5 and 10 mg, the heating rate was 10°C/min, the temperature was increased from 25°C to 1000°C and the gas flow rate was 50 ml/min.

### 2.8.6 Differential scanning calorimetry (DSC)

This analysis was helpful to determine the physical state of melatonin within the MSPs pores.

In DSC, the heat flow into and out of the system (i.e. melatonin loaded MCM-41) is measured as a function of temperature. Endothermic peaks in the DSC plot can be associated with melting, glass transition or, more rarely, decomposition. Exothermic peaks can indicate decomposition or molecular reorganization (e.g. crystallization).

DSC measurements were performed with a DSC 2010 Differential Scanning Calorimeter by TA Instruments. Data were collected and analysed with Advantage Software. The mass of the samples analysed varied between 3 and 5 mg and the nitrogen flow rate was 50 ml/min. The method used to heat the samples was the following: the temperature was increased from 20°C to 200°C (heating rate = 10°C/min), then maintained at 200°C for 15 minutes; subsequently, the temperature was decrease to 20°C (cooling rate = 10°C/min) and maintained at 20°C for 15 minutes; a second heating/cooling run was performed in the same way.

## 2.8.7 Dynamic Light Scattering (DLS)

DLS equipment was used to determine the MSPs zeta potential in suspension.

This technique can also be used to determine the hydrodynamic radius of particles. It utilizes a monochromatic laser, which is shot through a polarizer and into the sample. The scattered light is collected by a detector and it is analysed by the software using the Stokes Einstein relation. This equation is a model of Brownian motion based on random thermal motion which particles undergo while in suspension. The Stokes Einstein relation is the following:

$$D_h = \frac{k_B T}{3\pi\eta D_t} \qquad \text{(Eq.7)}$$

where $D_h$ is the hydrodynamic diameter (which represents the particle size), $D_t$ is the translational diffusion coefficient, $k_B$ is the Boltzmann's constant, T is the temperature and η is the dynamic viscosity.

To determine the zeta potential of the particles the microelectrophoresis function of the instrument was used.

DLS measurements were performed using a Malvern Zetasizer Nano ZS instrument, which can analyse particles with a size range between 0.3 nm and 10 μm with a 633 nm laser. Uncoated or PAA-coated particles in suspension were analysed at room temperature in disposable plastic cuvettes in SGF and SIF.

## 2.8.8 Fourier Transform Infrared Spectroscopy (FT-IR) Analysis

FT-IR is a technique used to identify compounds through their infrared spectrum of absorption of light, at different wavelength. The term Fourier Transform is related to the fact that this mathematical process is applied to the raw data to convey the final spectrum.

In infrared spectroscopy a beam of light containing many frequencies is shone at the sample and the instrument measures how much of that beam is absorbed by the sample. The beam is modified to contain different frequencies and a second data point is collected. The same process is repeated many times. Eventually a computer analyses the data in order to determine the absorption value at each wavelength.

The FT-IR instrument used in this project was Thermo Scientific Nicolet iS5 FT-IR Spectrometer with iD5 ATR accessory. Powders were measured without dilution.

# Chapter 3 – Results

## 3.1 Material Characterization

### 3.1.1 MCM-41

The mesoporous material MCM-41, synthesised and calcined according to the recipe in section 2.2, was characterised through XRD in order to verify its structure. As shown in Figure 9, the XRD curve presented three peaks at 2.27°, 4.02° and 4.63° in 2θ, representing the hexagonal (10), (11) and (20) reflections, respectively. These peaks confirmed the hexagonal mesoporous structure of the materials, since the ratio of $d_{10}/d_{11}$ is close to the theoretical value of $\sqrt{3}$ and $d_{10}/d_{20}$ is equal to 2 (Table 1a and b). The sharpness and intensity of the peaks are consistent with previously published data [71]. The materials were considered ordered enough to proceed with the experiments.

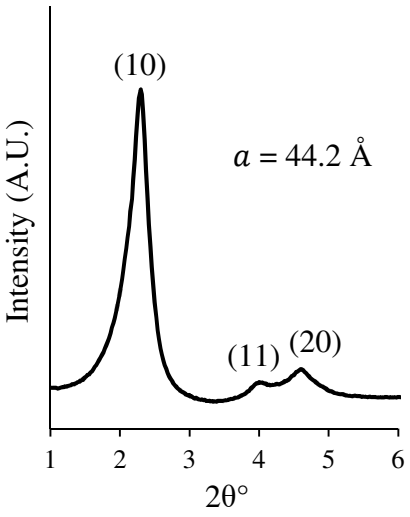


a)

| d | 2θ | hk |
|---|---|---|
| 38.3 | 2.31 | 10 |
| 21.5 | 4.12 | 11 |
| 18.8 | 4.69 | 20 |

b)

| Ratios | |
|---|---|
| $d_{10}/d_{11}$ | 1.8 |
| $d_{10}/d_{20}$ | 2.0 |

Figure 9. The XRD curve of calcined MCM-41 has three characteristic peaks. The unit cell *a* value can be calculated from the $d_{10}$ (38.3 Å).

Table 1. a) The values of the d-spacing for each peak with the corresponding 2θ value and Miller indices are reported; b) the ratios between the d-spacing were calculated: the hexagonal mesoporous structure was confirmed by these values.

The nitrogen adsorption isotherm measurements performed on the calcined MCM-41 revealed a specific surface area larger than 1000 m²/g (BET), a pore volume of 0.65 $cm^3/g$ and a pore diameter centred on 32.2 Å. No hysteresis was observed in the desorption branch of the isotherm (Figure

10a), due to the pore size (Figure 10b) being below the critical size in which nitrogen is able to form a condensed fluid layer within the pores, which is the basis for the hysteresis itself [72].

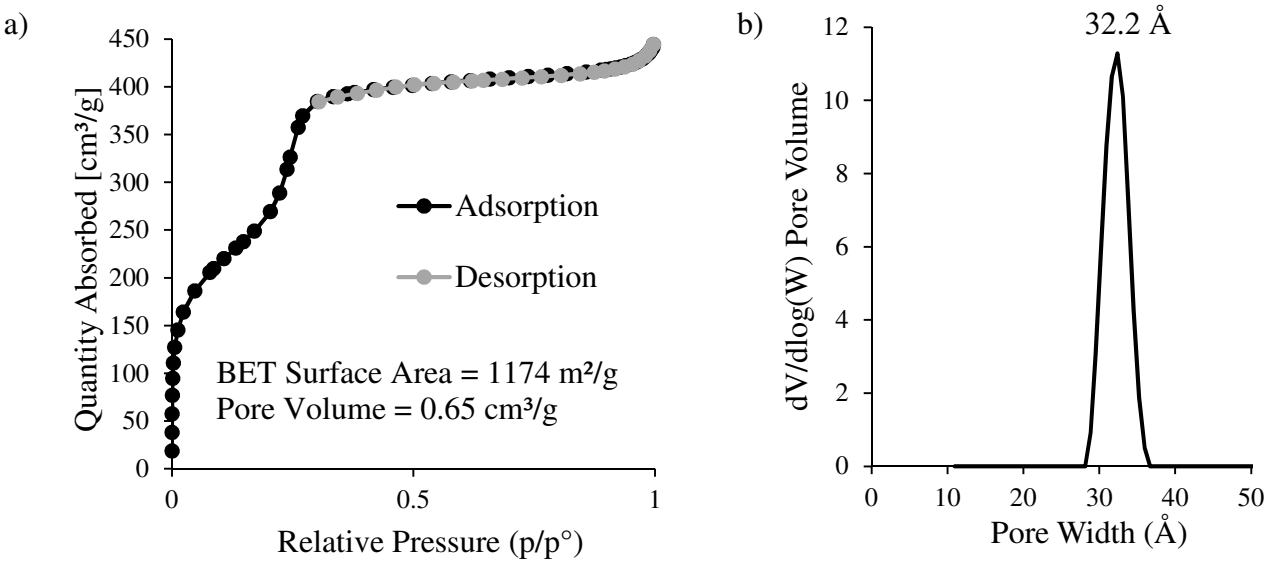


Figure 10. a) The calcined MCM-41 had a characteristic type IV isotherm curve. Capillary condensation occurred in a small relative pressure range, indicative of a sharp pore size distribution. The small increase in nitrogen adsorbed at the end of the plateau, at high relative pressure, was caused by gas adsorption in between mesoporous particles; b) the pore size distribution was centred on 32.2 Å.

The wall thickness can be evaluated by subtracting the pore diameter from the $d_{10}$ spacing, obtained from XRD. For these materials the wall thickness was calculated to be 6.1 Å.

SEM observations allowed to capture the particle shape and determine the dry particles size. MCM-41 presented a spheroidal shape (Figure 11a). The particle dimension was estimated to vary between 50 and 600 nm. Figure 11a shows aggregated particles, which could be due to the dry condition in which the sample was prepared for SEM observation. Some evidence of Ostwald ripening[†] [73] such as particle necking, can also be seen from SEM and TEM images which could affect particle aggregation and size distribution,. This is often observed for synthesis of colloidal particles under alkaline conditions and with hydrothermal treatment, such as those used for MCM-41.

The TEM image (Figure 11b) shows the pores of MCM-41 from two different directions. When the electrons go through the materials perpendicular to the pores channels, pores (lighter contrast areas) appear radially distributed inside the silica structure (darker contrast areas). When the electrons pass

[†] Ostwald ripening is defined as the dissolution and subsequent re-deposition of small crystals or sol particles on the surfaces of larger crystals or sol particles.

through MCM-41 parallel to the pores channels, the hexagonal arrangement of the pores is visible leading to white spots in the image.

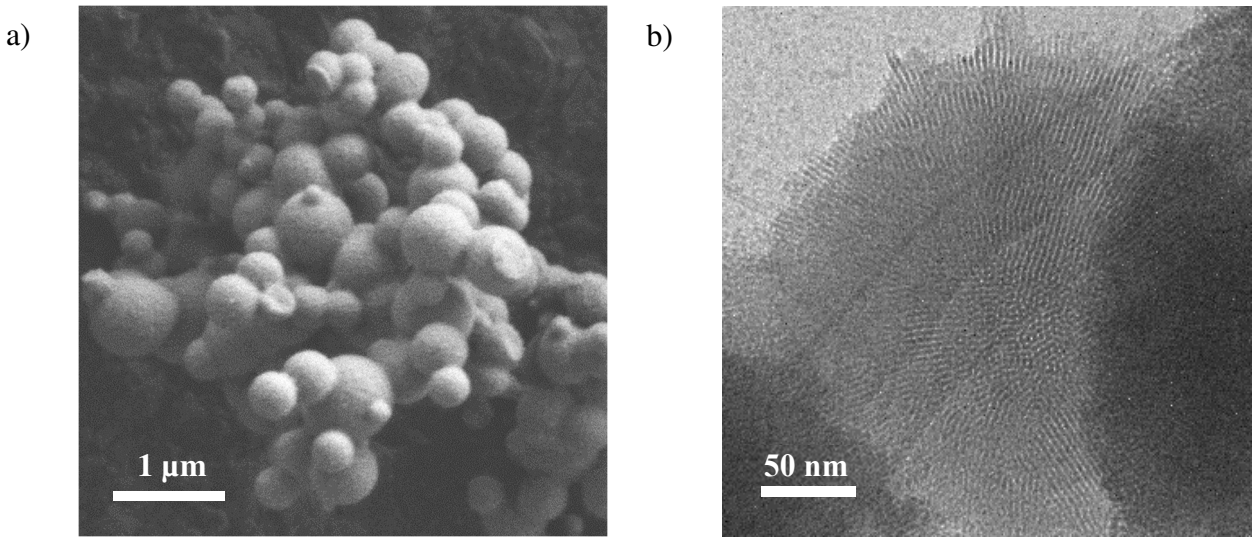


Figure 11. a) SEM image showing the spheroidal morphology and the dimension of calcined MCM-41 particles; b) MCM-41 image captured through TEM showing radially distributed pores and with an irregular particle surface.

Through the DLS equipment, microelectrophoresis measurements of the zeta potential were possible. In SIF (pH 6.8) the zeta potential of MCM-41 was -13.57 ± 0.74 mV, while in SGF (pH 1.2) it was +1.65 ± 0.22 mV, which was consistent with the fact that silica isoelectric point is at pH 2.

### 3.1.2 Melatonin-loaded MCM-41

After the loading of melatonin into MCM-41, the actual loading percentage was assessed through TGA measurements. The theoretical loading percentages, as described in section 2.3, were 10, 20 and 30 wt%. The final loadings were determined to be 7.7, 19.3, 22.9 wt%. Figure 12 shows a representative TGA curve for the sample with 19.3 wt% melatonin loading. The first weight loss was associated with solvent (ethanol) remaining in the materials after the drying step post-loading. The other two represented the two melatonin decomposition stages consistent with that observed for free melatonin (see suporting information Fig 33). The first one occurs between 226° C and 326° C, the second between 326° C and 741° C. This latter stage may include weight losses due to so-called framework water from uncondensed silanol groups within the silica wall (see section 3.4 for further

discussion). The decomposition of melatonin appears to shift to lower temperatures when confined within the mesoporous of MCM-41, as evidence by the lower temperature of the fist decomposition peak of loaded melatonin (292°C) versus that of the free melatonin (313°C). The decrease of the decomposition temperature of melatonin confined into the pores in comparison to that of the free hormone is thought to be the first evidence of the physical state of melatonin. The free hormone is crystalline, while the confinement of it inside the pores might prevent the formation of crystals, resulting in an amorphous state.

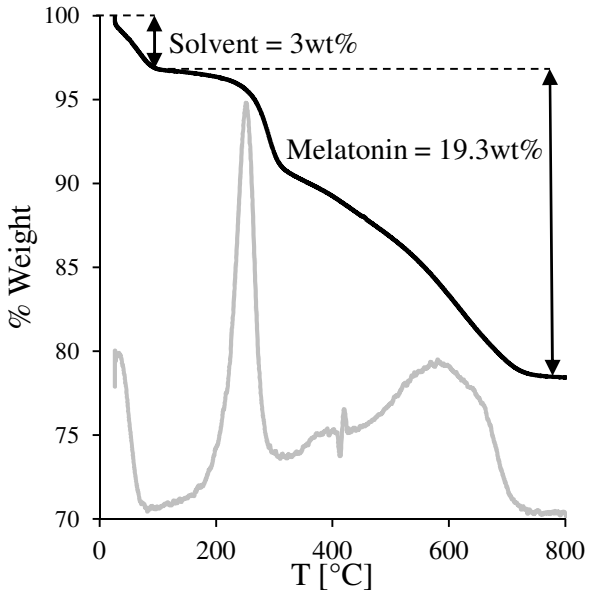


Figure 12. TGA curve of MCM-41 theoretically loaded with 20wt% of melatonin (black line). The first weight loss of 3 wt% is solvent still present in the materials, while the subsequent weight loss (19.3wt%) can be associated with a two step decomposition of the hormone, which can also be seen in the derivative curve (grey line).

XRD measurements were used in order to determine the physical state of the melatonin in the loaded MCM-41. The XRD curves of the melatonin loaded samples were compared to free melatonin. The free hormone was crystalline, and therefore showed the expected scattering peaks at high 2θ angle (atomic distances). In Figure 13 the curves of the three loaded samples were plotted together with the free melatonin. At lower loading percentages (7.7 and 19.3 wt%) no crystalline peaks are evident, indicative that the hormone was all in an amorphous state and, thus, presumably inside the pores. For the MCM-41 loaded with 22.9 wt% melatonin, some small scattering peaks that could be associated with crystalline melatonin were present at 24.22°, 24.88° and 26.19° (2θ).

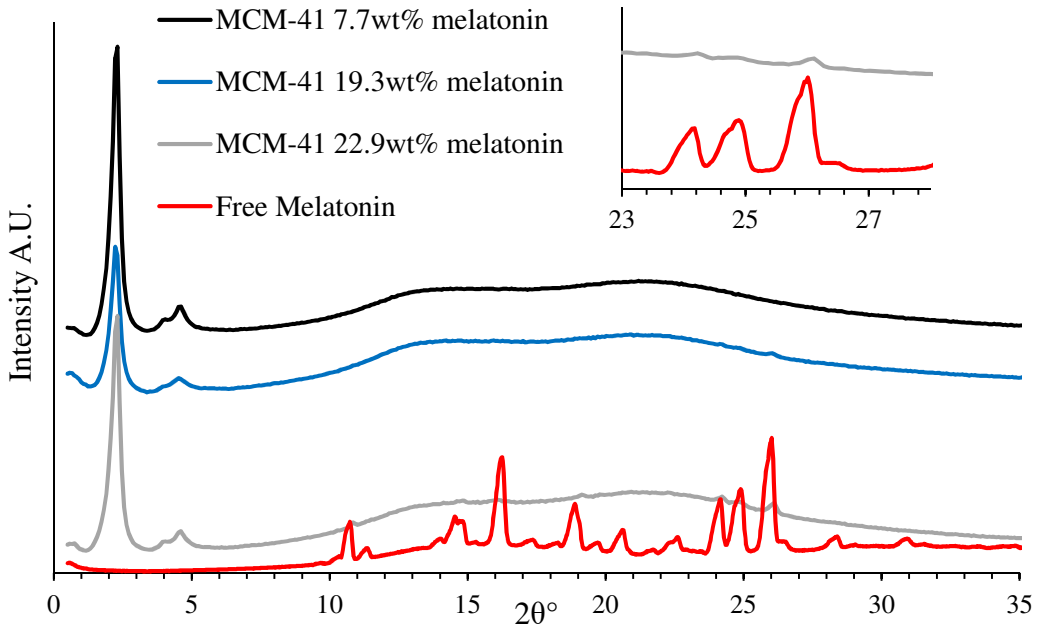


Figure 13. The XRD curves confirmed the presence of amorphous melatonin in MCM-41 loaded with 7.7 and 19.3 wt% of the hormone, and some indication of crystallization at a high loading of 22.9 wt%. Note that there was no change in the low angle region (1°-6° 2θ) due to hormone loading.

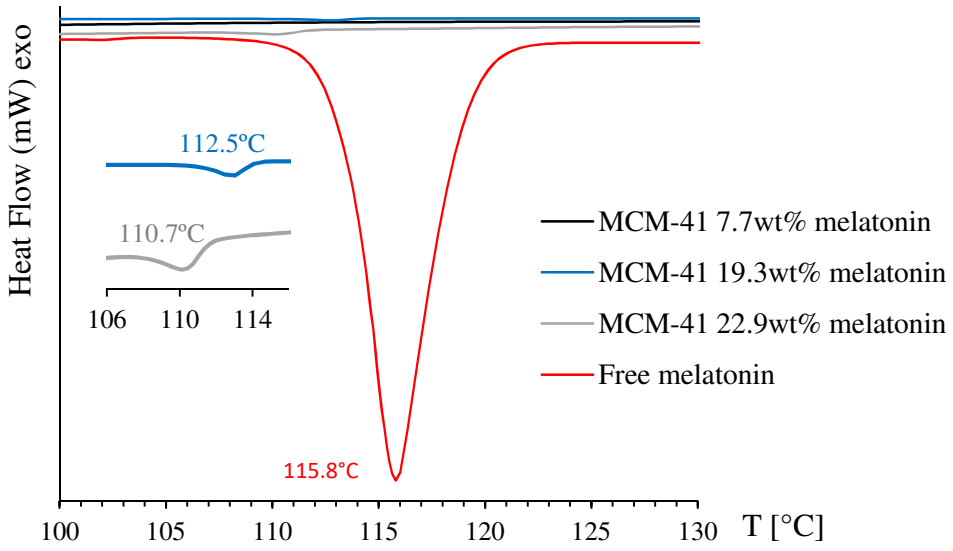


Figure 14. DSC curves showed a shift in the melting peak: free melatonin at 115.79°C, MCM-41 loaded with 22.9wt% melatonin at 110.72°C, MCM-41 with 19.3wt% at 112.50°C. No melting peak was present for MCM-41 loaded with 7.7wt%. The areas under the melting peaks represented the heat of melting and they were used to determine the percentage of crystalline melatonin.

In order to further confirm the physical state of the melatonin loaded in MCM-41, DSC measurements were performed and the free melatonin was compared to melatonin loaded into

MCM-41 (Figure 14). The thermal parameters melting temperature ($T_m$) and heat of melting ($\Delta H_m$) for free melatonin, MCM-41 with 7.7wt% melatonin, 19.3wt% melatonin and 22.9wt% melatonin are listed in Table 2.

| Sample | $T_m$ [°C] | $\Delta H_m$ [J/g] | % crystalline melatonin |
|---|---|---|---|
| MCM-41 7.7wt% melatonin | - | - | - |
| MCM-41 19.3wt% melatonin | 112.50 | 0.70 | 0.07 |
| MCM-41 22.9wt% melatonin | 110.72 | 0.92 | 0.10 |
| Free melatonin | 115.79 | 944.70 | 100 |

Table 2. There was a shift in the melting temperature towards lower values and a significant decrease in the heat of melting when melatonin was loaded into MCM-41. The percentage of crystalline hormone was estimated from the ratio of melting enthalpies of loaded and unloaded melatonin ($\Delta H_m$loaded/$\Delta H_m$crystalline).

Nitrogen adsorption isotherm was used to observe how surface area, pore volume and pore size changed with the increase of melatonin loading percentage. As can be seen in Figure 15, all three decreased with the increase of melatonin loading percentage. The pore volume of MCM-41 without melatonin was 0.65 $cm^3/g$, became 0.17 $cm^3/g$ when 22.9wt% melatonin was present. The initial pore size of MCM-41 (32.2 Å) decreased up to 12% with the loading of the hormone. The surface area went from 1174 $m^2/g$ when no melatonin was present in the sample to 318 $m^2/g$ with the highest loading percentage.

As the sample with 19.3wt% was the one with the highest loading percentage and lowest crystalline melatonin, it was chosen for the subsequent step of PAA coating and for the release measurements.

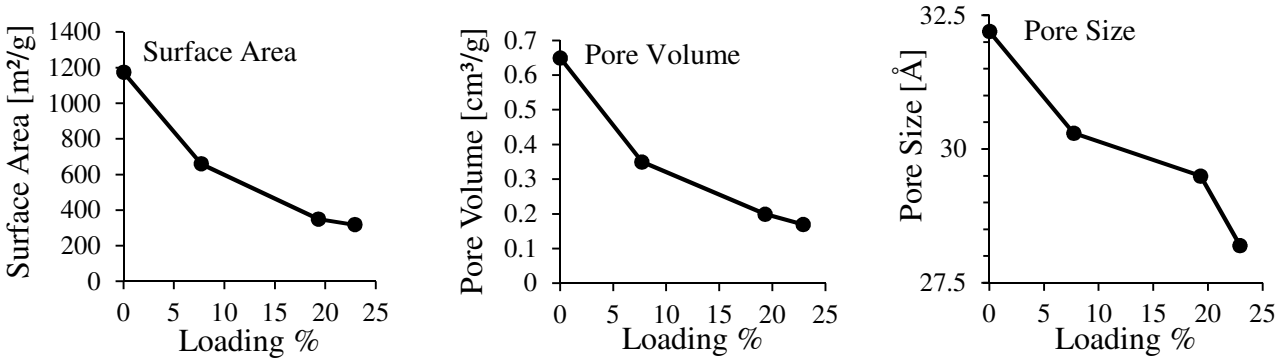


Figure 15. The surface area, pore volume and pore size reduction were signs of the presence of melatonin inside MCM-41 pores, as the pore space that is occupied by melatonin cannot be filled with nitrogen.

### 3.1.3 PAA-coated MCM-41 with melatonin

To assess the presence of PAA in the sample, FT-IR analysis was used. Figure 16a and b show the curves for free melatonin, MCM-41, MCM-41 with 19.3wt% melatonin, PAA and PAA-coated MCM-41 with 19.3wt% melatonin. Free melatonin presented peaks at 3290, 1620 and 1210 $cm^{-1}$ which could be associated with N-H, C=O and C-N stretching respectively (see Supporting Information, Figure 34). MCM-41 had a characteristic peak at 1060 $cm^{-1}$ that was due to the siloxane linkages. In melatonin loaded MCM-41 two peaks could be seen: one at 1620 $cm^{-1}$ which was the melatonin C=O group and one at 1060 $cm^{-1}$ that represented the Si-O-Si bonds (Figure 16a). The PAA curve presented two characteristic peaks: 1660 and 1420 $cm^{-1}$ which could be associated with C=O and COOH stretching, respectively. In the PAA-coated MCM-41 with melatonin curve, there were three characteristic peaks: the two of PAA and the siloxane one of MCM-41 (Figure 16b).

Nitrogen adsorption isotherm confirmed that the pores of MCM-41 were completely blocked by the PAA (Figure 17a), as no porosity was measured by the instrument. It was assumed that the PAA was present only on the surface of the particles. Its average molecular weight was 1800 making it unlikely for it to diffuse within the 32 Å pores of MCM-41. TEM observations (Figure 17b) of the PAA-coated MCM-41 showed no difference in comparison to the uncoated sample. The contrast of the PAA coating was not enough in comparison to the MCM-41 to be evident, so it appeared transparent.

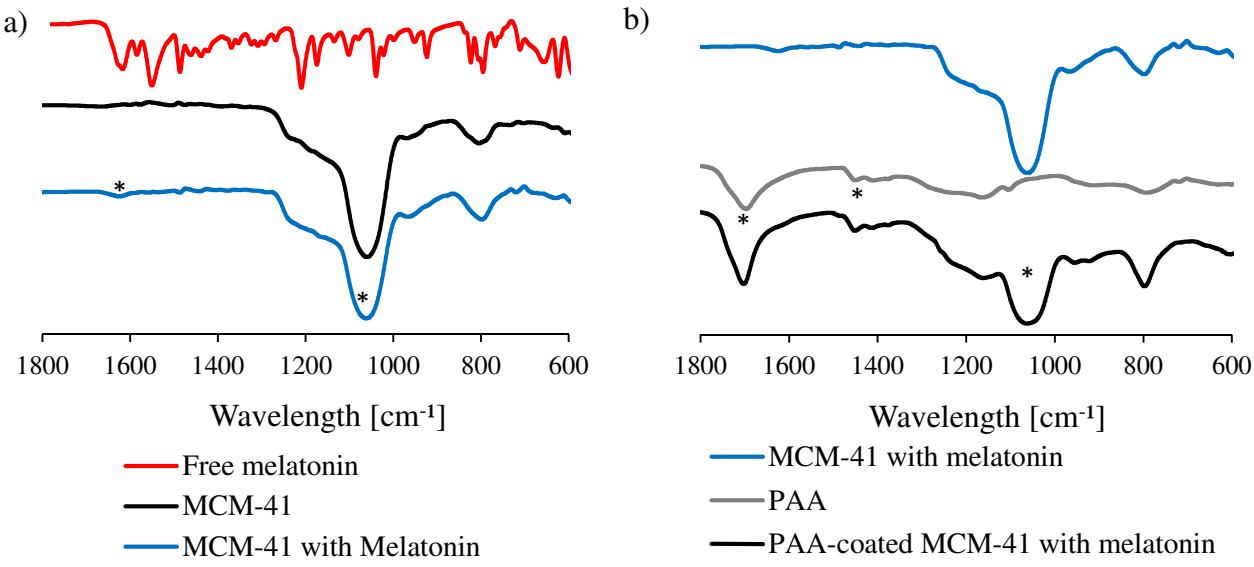


Figure 16. a) In melatonin loaded MCM-41 curve a peak associated with melatonin at 1620 $cm^{-1}$ and a peak at 1060 $cm^{-1}$ typical of siloxane bonds can be seen. b) In the PAA-coated curve it is possible to notice two peaks associated with PAA (1660 and 1420 $cm^{-1}$) and the peak of siloxane bonds (1060 $cm^{-1}$).

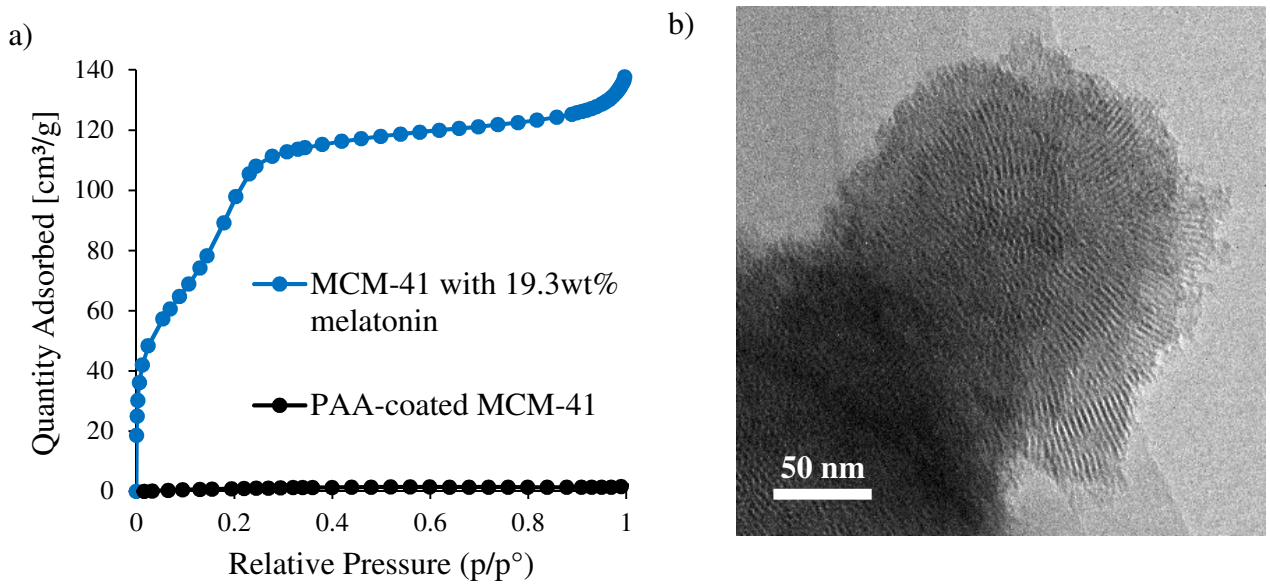


Figure 17. a) Nitrogen adsorption curves for melatonin loaded MCM-41 before and after coating with PAA. Uncoated MCM-41 with melatonin retains its porosity as evidenced from a capillary condensation step between 0.2-0.3 in relative pressure. No evidence of porosity is shown in the PAA-coated sample; b) it was not possible to see contrast from the polymeric coating around the particles on the basis of TEM.

SEM image (Figure 18) shows agglomerated particles of MCM-41 embedded in PAA. The polymer formed a matrix in which the MCM-41 particles containing melatonin were trapped. There was no apparent control over the thickness of the PAA layer.

TGA analysis was used in order to verify the ratio of PAA present in the coated MCM-41. As described in Section 2.4, the theoretical weight ratio was melatonin loaded MCM-41: PAA 1:2. From Figure 19 it can be seen that there was an initial weight loss of about 3wt% that was associated with solvent absorbed by the sample. The second weight loss could be occluded solvent, or rather solvent which was not removed during the process of coating. The peaks between 163°C and 700°C represented both melatonin and PAA. The overlapping between the peaks of the hormone and the ones of the coating did not allow to confirm the exact ratio of PAA present into the sample. Moreover, for the same reason, it was not possible to assess the presence of the same amount of melatonin initially present inside the materials (19.3 wt%). Microelectrophoresis measurements conducted in SIF (pH 6.8) revealed the zeta potential of the particles was -16.90 ± 1.38 mV and in SGF (pH 1.2) it was +5.86 ± 0.53 mV.

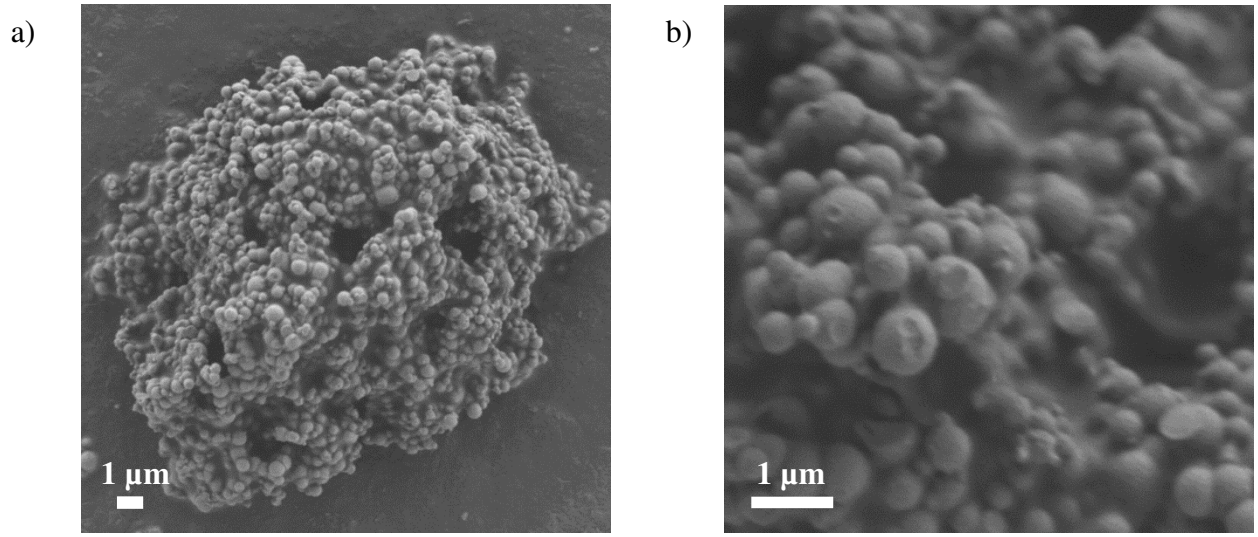


Figure 18. SEM images at different magnification: a) x 4,000 and b) x 15,000. MCM-41 particles appeared embedded into PAA, even if some of them might not be completely covered with the polymer. The overall sample seemed to consist of big clumps of PAA with MCM-41 entrapped in it.

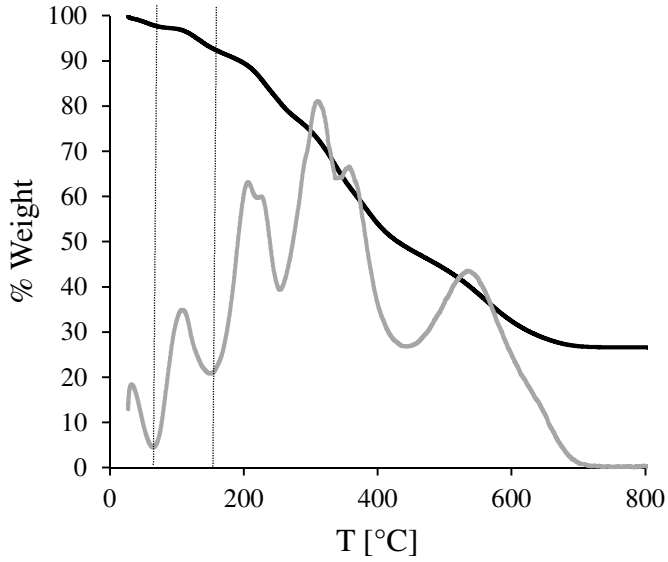


Figure 19. TGA curve of PAA-coated MCM-41 with melatonin presented many peaks between 163°C and 700°C which were associated with PAA and melatonin. The overlapping of the peaks of the two compounds prevented from confirming the ratio of polymer and the percentage of the hormone in the sample.

## 3.2 Dissolution

The aim of this project was to test the release of melatonin from MCM-41 particles coated with PAA in SGF and SIF under sink conditions. A comparison with free melatonin and Circadin was also important to understand the properties of the new formulation.

### 3.2.1 Circadin release profiles in SGF and SIF

Dissolution profiles of free melatonin and Circadin in SGF (pH 1.2) and SIF (pH 6.8) were carried out in order to use them as reference points for the study of the PAA-coated MCM-41 with melatonin.

In SGF, Figure 20 shows that the Circadin pill slowed down the release of melatonin in comparison to both the crushed pill and the free melatonin. Free melatonin and crushed Circadin reached plateau after 30 minutes, whereas the Circadin pill reached plateau after 10 hours. Table 3 shows the dissolution constants for Circadin and melatonin.

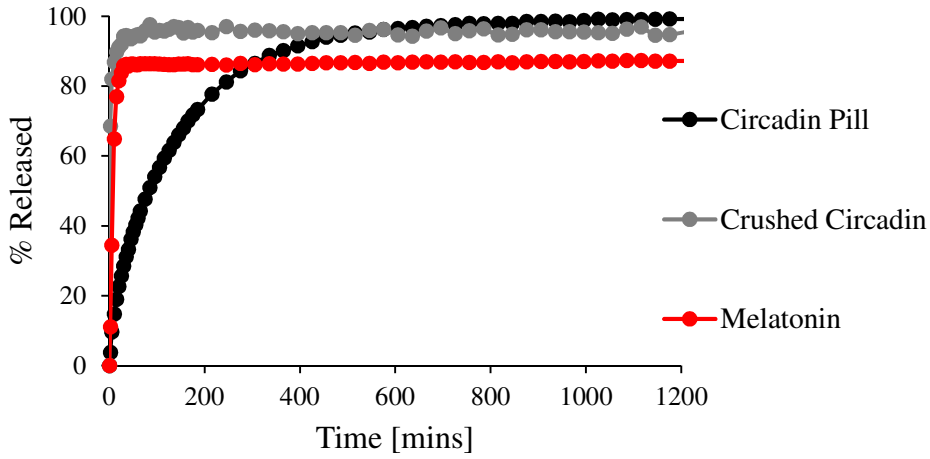


Figure 20. In SGF Circadin significantly delayed the release of melatonin, reaching 100% of release (which corresponds to 2 mg) after approximately 10 hours from the beginning of the measurement. After 30 minutes, crushed Circadin and free melatonin had both reached 100% release, while Circadin pill released only 28.5% of the melatonin in it.

a)

| Sample | Higuchi Dissolution Constant (kH) | $R^2$ | T-lag |
|---|---|---|---|
| Circadin pill | 13.2 | 0.9592 | 1.8 |
| Crushed Circadin | 48.1 | 0.9405 | 0.0 |

b)

| Sample | First-order Dissolution Constant (k1) | $R^2$ |
|---|---|---|
| Free melatonin | 0.1 | 0.9880 |

Table 3. a) Higuchi dissolution constants for Circadin revealed the difference between the intact pill and the crushed one: when crushed the formulation lost his delayed properties and the rate constant is almost tripled, so the rate of release is much higher; b) free melatonin (powder) followed a first-order dissolution profile.

In the SIF neutral environment, Circadin released melatonin at a lower rate compared to SGF. The free hormone reached its maximum percentage released after 20 minutes, the crushed Circadin after 30 minutes, while the Circadin pill reaches plateau in about 20 hours (Figure 21a and b).

At neutral pH Circadin pill dissolution constant decreased of about 24% in comparison to the one in acidic conditions. Crushed Circadin dissolution constant is similar in the two conditions, while free melatonin dissolution constant increases in SIF (Table 4).

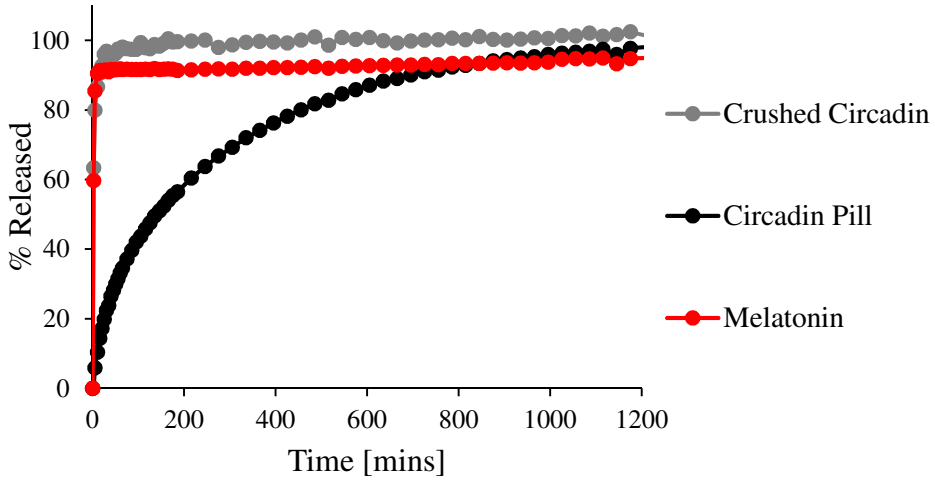


Figure 21. In SIF the release of melatonin from the Circadin pill is slower than the one in SGF. The pill reached 100% release after 20 hours. After 30 minutes, crushed Circadin and free melatonin had both reached 100% release, while Circadin pill released only 22% of the melatonin in it.

a)

| Sample | Higuchi Dissolution Constant (kH) | $R^2$ | T-lag |
|---|---|---|---|
| Circadin pill | 10.0 | 0.9936 | 1.9 |
| Crushed Circadin | 46.0 | 0.9683 | 0.0 |

b)

| Sample | First-order Dissolution Constant (k1) | $R^2$ |
|---|---|---|
| Free melatonin | 0.4 | 0.9317 |

Table 4. a) Higuchi dissolution constant for Circadin pill decreased of almost 25% in SIF compared to SGF. The dissolution constant of the crushed Circadin is similar to the one in SGF; b) the first-order constant of free melatonin increased four times in comparison to the acidic environment.

Circadin delayed the release of melatonin in both acidic (SGF) and neutral (SIF) conditions with some differences in the two environments. When crushed Circadin lost his delay release property and a burst release of the hormone could be seen in both pH conditions.

### 3.2.2 PAA-coated MCM-41 with 19.3 wt% melatonin

Release measurements of melatonin from MCM-41, PAA-coated MCM-41 and only PAA were performed using cellulose capsules to drop the samples in the dissolution vessels. The capsules did not affect the release results as they were completely dissolved after few minutes.

In the acidic environment of SGF, the release of melatonin from MCM-41, PAA-coated MCM-41 and only PAA did not seem to reach a plateau (Figure 22). Moreover, the absorbance values were not comparable to the ones of Circadin and it was not possible to determine the amount and the percentage of melatonin released from the different samples. It was hypothesised an interference of the PAA and/or the silica particle with the UV-Vis measurements (see Supporting Information, Figures 35 and 36).

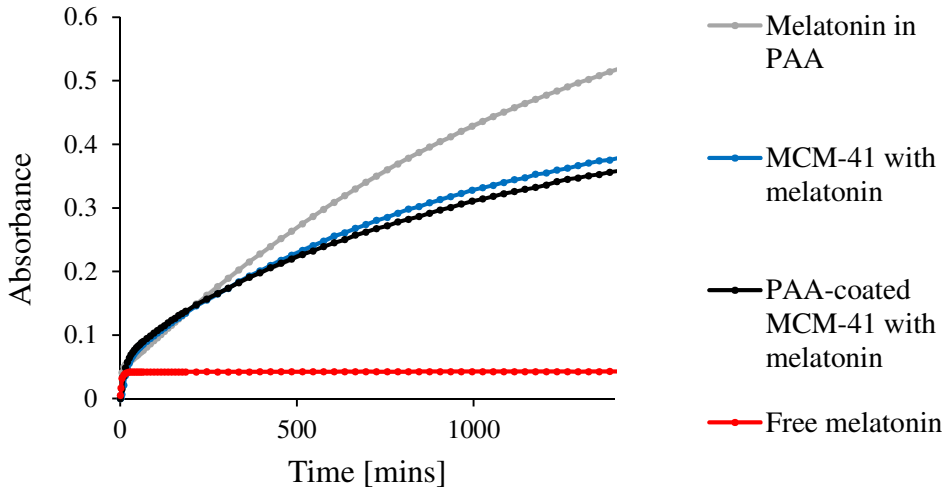


Figure 22. After 24 hours absorbance curves did not reached plateau and the absorbance values were very different from the ones of Circadin, so the amount released could not be calculated and, consequently, no percentage release could be determined.

In SIF free melatonin had the faster rate of dissolution compared to the other samples. Melatonin only embedded in PAA and uncoated MCM-41 with melatonin had a very similar dissolution constant (Table 5). PAA-coated MCM-41 slowed down the release of melatonin compared to the uncoated ones, presenting a dissolution constant almost 25% lower than the uncoated MCM-41. So, the combination of PAA and MCM-41 is essential to slow down the release of melatonin, whilst the

use of only one of the two is less efficient. The slowest formulation is Circadin (intact pill) (Figure 23). The fact that some samples reached more than 100% release might be due to some experimental errors, during the weighing procedure for example.

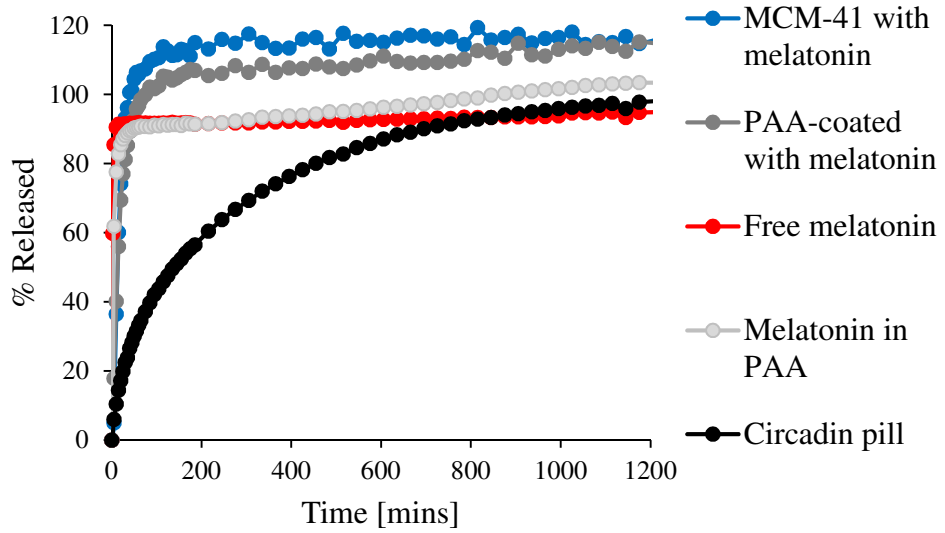


Figure 23. a) PAA-coated MCM-41 slowed down the release of melatonin in comparison to free melatonin, melatonin embedded in PAA and uncoated MCM-41, but presented a faster release in comparison to Circadin; b) after 30 minutes free melatonin and melatonin in PAA had reached plateau, uncoated MCM-41 had released 93% of melatonin, PAA-coated MCM-41 had released 81% of the melatonin and Circadin only 22%.

| Sample | Higuchi Dissolution Constant (kH) | $R^2$ | T-lag |
|---|---|---|---|
| MCM-41 with melatonin | 58.8 | 0.9953 | 2.8 |
| PAA-coated MCM-41 with melatonin | 44.3 | 0.9926 | 2.1 |
| Melatonin in PAA | 56.3 | 0.9651 | 1.4 |

Table 5. Melatonin in PAA and MCM-41 without any coating had a similar Higuchi dissolution constant, while PAA-coated MCM-41 presented a dissolution constant almost 25% lower than uncoated MCM-41.

The comparison between the formulation designed in this project and Circadin did not take into account that the first one is a powder, whilst the second is a pill. As it was confirmed by the crushed Circadin release profile, the way Circadin is pelletized made a significant difference in delaying the release of melatonin. PAA-coated MCM-41 with melatonin had a similar Higuchi dissolution constant of crushed Circadin, but more than four times higher than the Circadin pill.

## 3.3 Biological Assays

### 3.3.1 Apoptosis

Apoptosis was chosen as a preliminary test to determine the effect of free melatonin, MCM-41 without melatonin, uncoated and PAA-coated MCM-41 with melatonin at different concentrations on the viability of murine BV2 cells. MCM-41 at 50 µg/ml treatment for 24 hours significantly decreased the percentage of live cells and increased early apoptotic one compared to the negative control. No statistically significant difference for late apoptotic cells and dead cells percentage. No significant difference was found for MCM-41 at 100 µg/ml compared to the negative control, apart from the early apoptotic percentage which increased (Figure 24). No statistically significant difference was found for any of the MCM-41 with melatonin samples in comparison to the negative control (Figure 25). For PAA-coated MCM-41 with melatonin the only significant differences could be found at 100 µg/ml for the live and early apoptotic values (Figure 26). No significant difference between melatonin and the negative control was found (Figure 27).

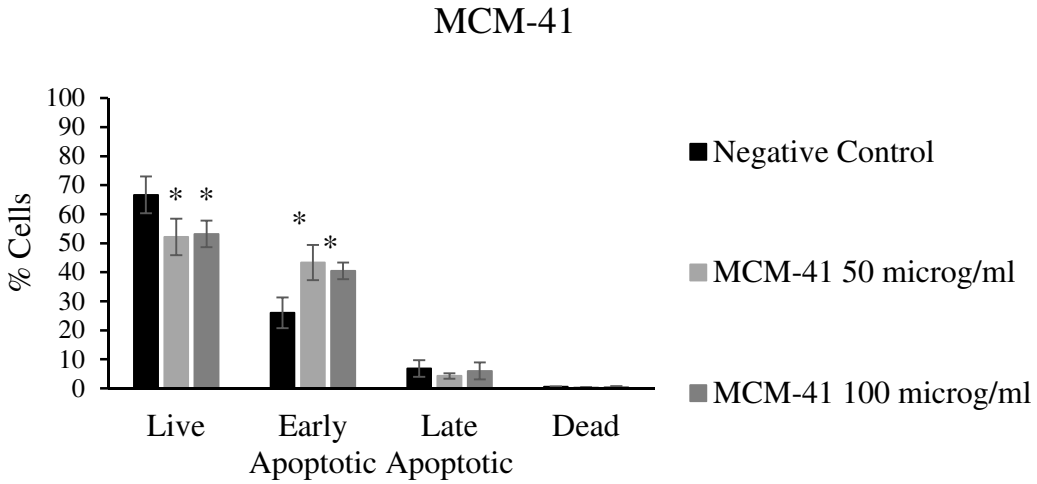


Figure 24. MCM-41 50 and 100 µg/ml appear to similarly reduce the number of alive cells and increase the number of early apoptotic cells in comparison to the negative control. No significant difference was assessed for late apoptotic and dead cells.

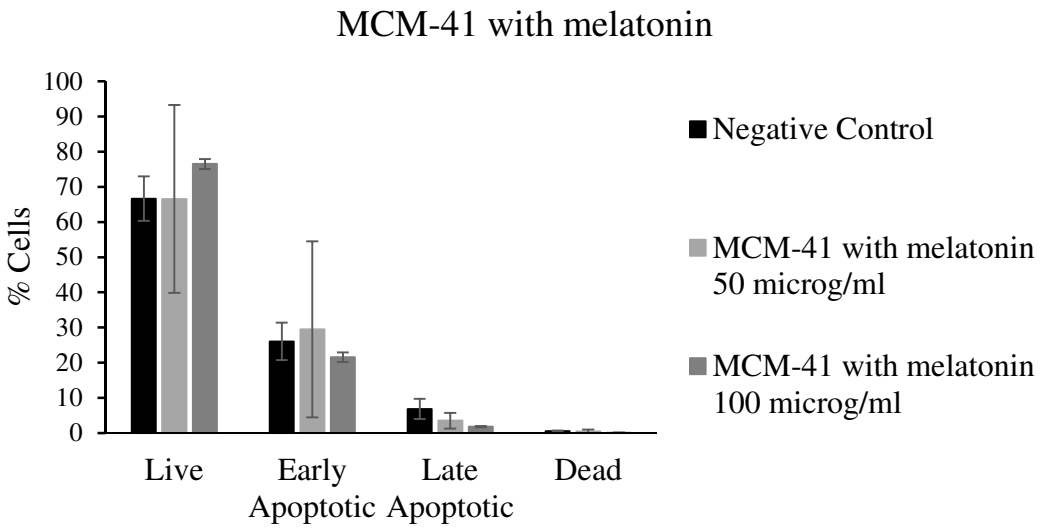


Figure 25. Both samples of MCM-41 with melatonin (50 and 100 µg/ml) had no significant impact on cells viability. No difference was found for any of the cells stages studied (live, early apoptotic, late apoptotic and dead) between the melatonin loaded particles and the negative control.

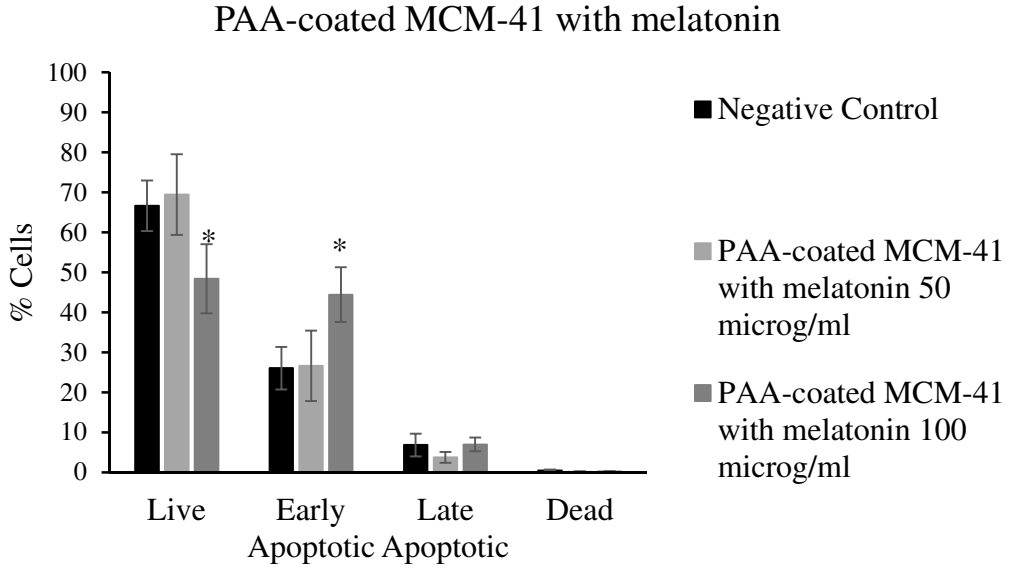


Figure 26. PAA-coated MCM-41 appeared to decrease the percentage of alive cells and increase the early apoptotic ones only at the highest concentration (100 µg/ml).

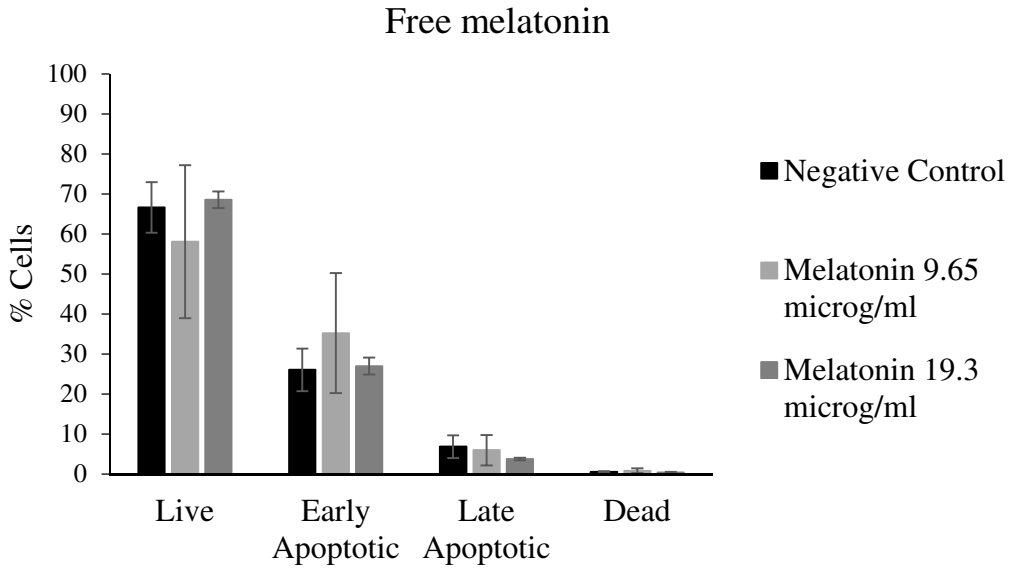


Figure 27. Melatonin was used as a control and it did not show to affect cell viability in any way in comparison to the negative control.

In the figures one star (*) represents a p value lower than 0.05, two stars (**) a p value lower than 0.01 and three stars (***) a p value lower than 0.001. MCM-41 without melatonin decreased the percentage of alive cells and increased the one of early apoptotic at both concentrations tested (50 and 100 µg/ml) in comparison to the negative control (no treatment). However, they did not affect the percentage of late apoptotic and dead cells. MCM-41 with melatonin did not affect the cells in comparison to the negative control. PAA-coated MCM-41 with melatonin decreased the alive cells and increased the early apoptotic ones at both concentrations but had no effect on the late apoptotic and dead cells. Melatonin had no significant effect on the cells in comparison to the negative control. Overall, uncoated and PAA-coated MCM-41 had no significant effect on murine BV2 cells apoptosis.

The apoptosis assay results revealed that the positive control used (LPS, concentration = 1 µg/ml) was not statistically significantly different from the negative control suggesting the positive control did not work as such (see Supporting Information, Figure 37).

### 3.3.2 ROS production

ROS assay was used to determine if the murine BV2 cells were stressed by the presence of the free melatonin, MCM-41 without melatonin, uncoated and PAA-coated MCM-41 with melatonin. MCM-41 alone at both concentrations (50 and 100 µg/ml) significantly decreased ROS production in comparison to the negative control (Figure 28). Melatonin loaded MCM-41 appeared to significantly decrease ROS production only at high concentration (Figure 29), while no significant difference was found for PAA-coated MCM41 with melatonin (Figure 30). Free melatonin significantly increased ROS production with a concentration equal to 9.65 µg/ml (Figure 31).

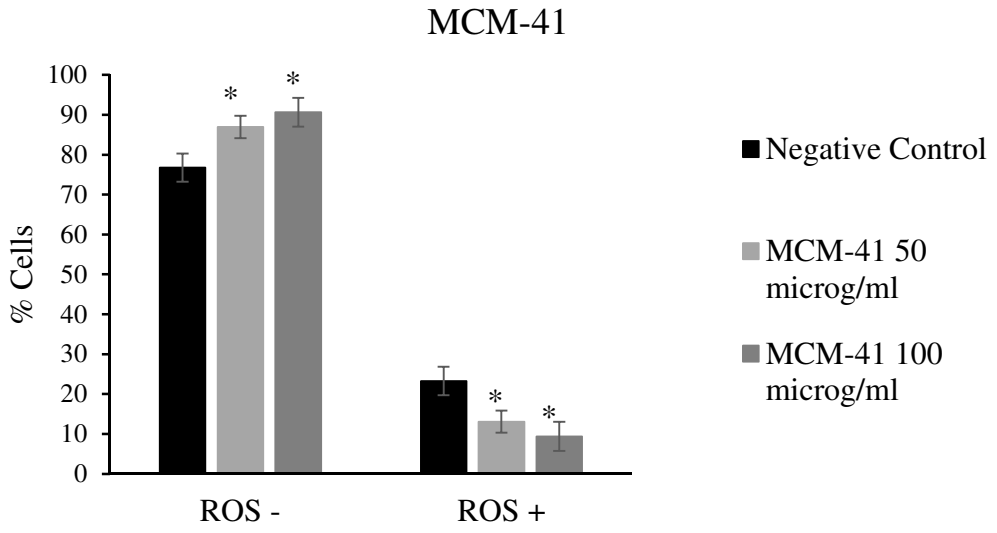


Figure 28. MCM-41 increased the % of ROS positive cells for both tested concentrations and this difference is significant according to the T-test performed on the data.

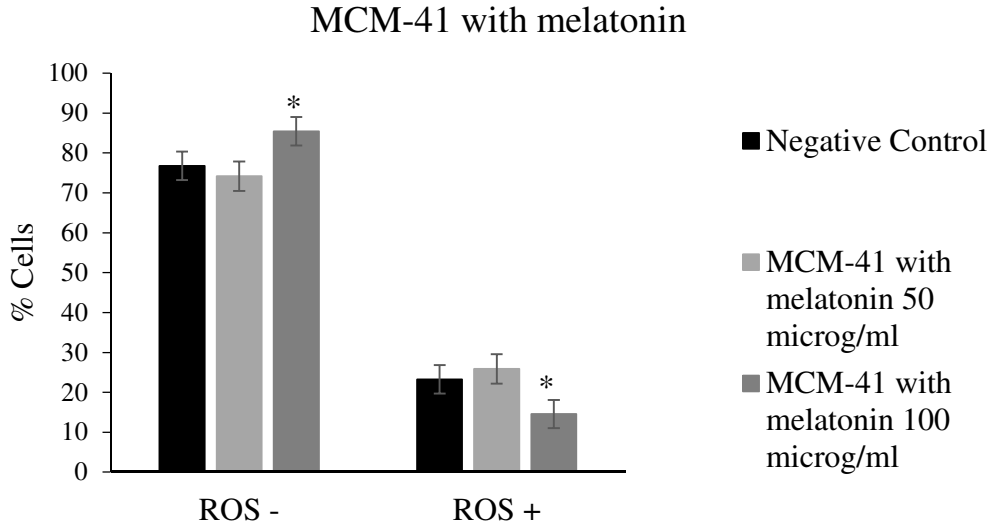

Figure 29. Melatonin loaded MCM-41 at 100 µg/ml significantly decreased the % of ROS positive cells.

.

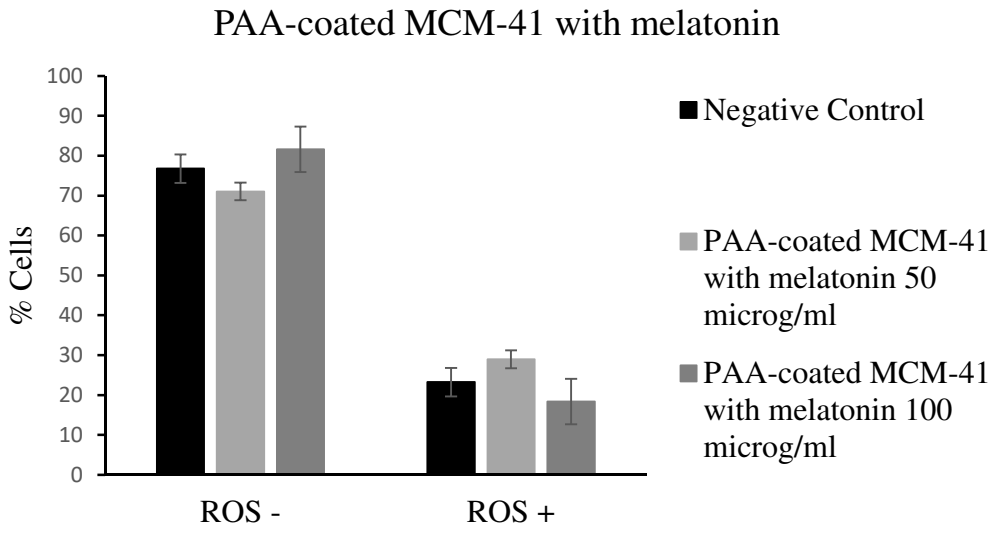


Figure 30. PAA-coated MCM-41 did not show any significant difference in inducing or suppressing ROS production in comparison to the negative control.

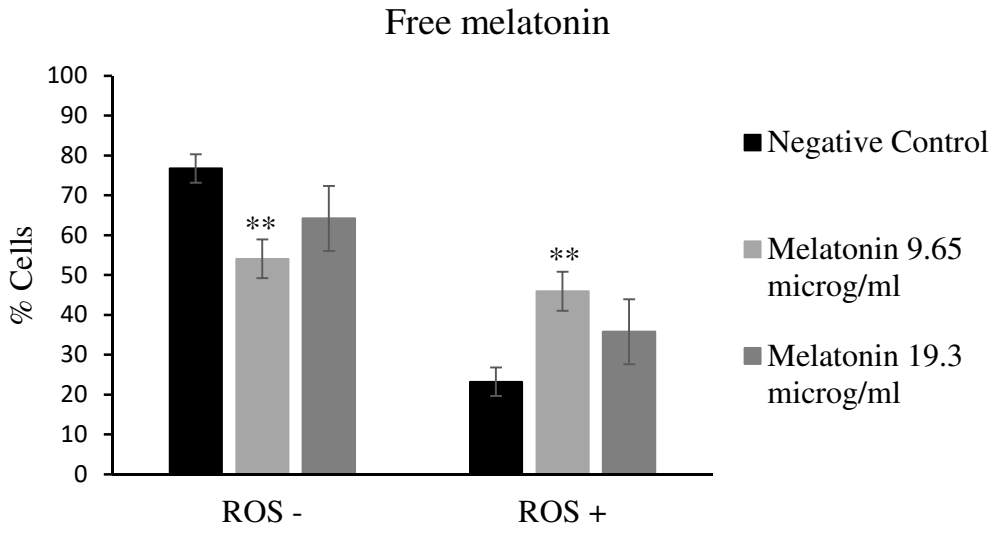


Figure 31. Melatonin was used as a control and at 9.65 µg/ml it seemed to significantly increase the percentage of ROS positive cells in comparison to the negative control.

In the figures one star (*) represents a p value lower than 0.05, two stars (**) a p value lower than 0.01 and three stars (***) a p value lower than 0.001. The results suggested that MCM-41 without melatonin decreased ROS positive cells percentage at both concentrations tested (50 and 100 µg/ml) compared to the negative. MCM-41 with melatonin decreased ROS production only at the highest concentration, while PAA-coated MCM-41 with melatonin had no effect on the ROS production in comparison to the negative control. Melatonin appeared to increase ROS production at lower concentration (9.65 µg/ml). Overall, uncoated and PAA-coated MCM-41 did not increase ROS production in murine BV2 cells.

The ROS assay results showed no statistically significant difference between the positive and negative control, LPS did not affect the cells ROS production (see Supporting Information, Figure 38).

## 3.4 Potential sources of error

a. From the TGA curve of melatonin loaded MCM-41 (Figure 12) it was calculated that a weight loss of 19.3% was associated with melatonin decomposition. However, part of the second decomposition step might be due to the loss of framework water present into MCM-41. MCM-41 TGA curve (Supporting Information, Figure 32) shows an initial weight loss of 2 wt% associated with moisture absorbed by the materials and a second weight loss of around 1 wt% which can be associated with framework water. Melatonin TGA curve (Supporting Information, Figure 33) shows that the second decomposition step of melatonin is between 448° and 558° C. Instead, for melatonin loaded MCM-41 curve (Figure 8) the second decomposition step occurs between 324° and 749° C.

b. PAA interference with UV-Vis measurements during the release measurements might have occurred. As shown in the Supporting Information – Figure 36, when PAA and melatonin are both dissolved in the same sample, an increase in the absorbance is measured. This might have distorted the results, resulting in the calculation of a slightly higher amount of melatonin than the actual one released from the particles. This was particularly significant for the release SGF media.

# Chapter 4 - Conclusions

The aim of this project was to design formulations for the release of melatonin using mesoporous silica materials and a polymeric coating. MCM-41 was synthesised and characterised using different physicochemical techniques. The materials appeared to have a spheroidal shape with dimension varying from 50 to 600 nm, high surface area (1174 $m^2/g$), large pore volume (0.65 $cm^3/g$) and pore size of 32.2 Å. MCM-41 were subsequently loaded with three different weight percentage of melatonin (7.7, 19.3 and 22.9 wt%) and the physical state of the hormone were assessed. As the sample with 19.3wt% presented the highest loading with the lowest crystallinity it was chosen to continue the study. MCM-41 particles with melatonin were coated with polyacrylic acid (PAA) and the presence of particles embedded in the polymer was confirmed.

Release measurements were performed in SGF (pH 1.2) and SIF (pH 6.8) in a dissolution apparatus under sink conditions for free melatonin, Circadin (crushed and pill), uncoated and PAA-coated MCM-41 with melatonin. Free melatonin presented a very fast dissolution rate in both environments with a first-order release profile. Circadin pills delayed the release of melatonin in both acidic and neutral conditions with a slower release rate in SIF. When crushed, Circadin lost its delay release property and a faster release of the hormone could be seen in both pH conditions. For uncoated and PAA-coated MCM-41 it was not possible to assess the release percentage of melatonin in SGF. In SIF PAA-coated MCM-41 with melatonin significantly changed the release profile of the hormone. They presented a Higuchi dissolution constant 25% lower than uncoated MCM-41 and very similar to that of crushed Circadin, which is approximately 4 times higher than Circadin pill dissolution constant. It must be noted that the formulation designed in this project was tested for the release of melatonin as a powder and compared to an available formulation, Circadin, which is a pill. This difference affected the release rate of the hormone and has to be taken into account when analysing the results.

Preliminary biological assays were performed in order to test the effect of uncoated and PAA-coated MCM-41 with melatonin. MCM-41 alone, MCM-41 with melatonin and PAA-coated MCM-41 at two different concentrations (50 and 100 µg/ml) were added to mouse microglial cells (BV2) and the cells were incubated with the particles for 24 hours. The apoptosis assay was used to obtain information about the viability of the cells, while the ROS production assay was used to determine if the formulation could cause stress to the cells. For apoptosis no statistically significant increase in the percentage of late apoptotic and dead cells was assessed for any sample at both concentrations tested. For ROS production no statistically significant increase in the ROS positive percentage of

cells was measured for the formulation at both concentrations. An increase in ROS production was present for free melatonin at the lower concentration (9.65 µg/ml).

# Chapter 5 – Future Work

The future work should focus on the improvement of different aspects of the formulation designed in this project, for example:

- synthesis of mesoporous silica materials with higher pore volume to host a larger amount of melatonin;
- more efficient loading method to avoid melatonin loss during drying process;
- more precise characterization of the PAA-coating: MCM-41:PAA weight ratio, thickness of the polymeric layer, single particle layer;
- investigation of release measurements in SGF and possible interference of PAA in the UV-Vis analysis or other sources of errors;
- confirmation of biological assays over wider concentrations and further immunotoxicological studies (i.e. cytokines production and genes expression);
- studies on the effects of PAA-coated MCM-41 with melatonin on the circadian rhythms of cells, e.g. Lumicycle. The Lumicycle equipment (Lumicycle32) allows to test the efficacy of formulations on the molecular circadian clock, through real-time luciferase recordings for biological rhythms assessment on tissues or cells. Thus, it is possible to study the differential effects of the melatonin formulation depending on the status of the cell culture previously synchronized.

# References


1. Soler-Illia, G.J.d.A., et al., *Chemical strategies to design textured materials: from microporous and mesoporous oxides to nanonetworks and hierarchical structures.* Chemical reviews, 2002. **102**(11): p. 4093-4138.
2. Kresge, C.T., et al., *The discovery of ExxonMobil's M41S family of mesoporous molecular sieves.* Studies in Surface Science and catalysis, 2004. **148**: p. 53-72.
3. Vincent, C., *Process for producing low-bulk density silica*. 1971, Google Patents.
4. Yanagisawa, T., et al., *The preparation of alkyltriinethylaininonium–kaneinite complexes and their conversion to microporous materials.* Bulletin of the Chemical Society of Japan, 1990. **63**(4): p. 988-992.
5. Beck, J., et al., *A new family of mesoporous molecular sieves prepared with liquid crystal templates.* Journal of the American Chemical Society, 1992. **114**(27): p. 10834-10843.
6. Kresge, C., et al., *Ordered mesoporous molecular sieves synthesized by a liquid-crystal template mechanism.* nature, 1992. **359**(6397): p. 710-712.
7. Attwood, D. and A.T. Florence, *FASTtrack Physical Pharmacy*. 2012: Pharmaceutical Press.
8. Atluri, R., N. Hedin, and A.E. Garcia-Bennett, *Nonsurfactant Supramolecular Synthesis of Ordered Mesoporous Silica.* Journal of the American Chemical Society, 2009. **131**(9): p. 3189-+.
9. Wan, Y. and D. Zhao, *On the controllable soft-templating approach to mesoporous silicates.* Chemical reviews, 2007. **107**(7): p. 2821-2860.
10. Pond, S.M. and T.N. Tozer, *First-pass elimination basic concepts and clinical consequences.* Clinical pharmacokinetics, 1984. **9**(1): p. 1-25.
11. Garcia-Bennett, A.E., *Synthesis, toxicology and potential of ordered mesoporous materials in nanomedicine.* Nanomedicine, 2011. **6**(5): p. 867-877.
12. Vallet-Regi, M., et al., *A new property of MCM-41: drug delivery system.* Chemistry of Materials, 2001. **13**(2): p. 308-311.
13. Slowing, I.I., et al., *Mesoporous silica nanoparticles as controlled release drug delivery and gene transfection carriers.* Advanced drug delivery reviews, 2008. **60**(11): p. 1278-1288.
14. Slowing, I.I., et al., *Mesoporous silica nanoparticles for drug delivery and biosensing applications.* Advanced Functional Materials, 2007. **17**(8): p. 1225-1236.
15. Popovici, R., et al., *Controlled drug delivery system based on ordered mesoporous silica matrices of captopril as angiotensin-converting enzyme inhibitor drug.* Journal of pharmaceutical sciences, 2011. **100**(2): p. 704-714.
16. Vallet-Regí, M., *Nanostructured mesoporous silica matrices in nanomedicine.* Journal of internal medicine, 2010. **267**(1): p. 22-43.
17. Song, S.-W., K. Hidajat, and S. Kawi, *pH-controllable drug release using hydrogel encapsulated mesoporous silica.* Chemical communications, 2007(42): p. 4396-4398.
18. Rosenholm, J.M., C. Sahlgren, and M. Lindén, *Towards multifunctional, targeted drug delivery systems using mesoporous silica nanoparticles–opportunities & challenges.* Nanoscale, 2010. **2**(10): p. 1870-1883.
19. Barahona, F., et al., *Multimethod approach for the detection and characterisation of food-grade synthetic amorphous silica nanoparticles.* Journal of Chromatography A, 2016. **1432**: p. 92-100.
20. European Parliament and Council Directive No 95/2/EC of 20 February 1995 on food additives other than colours and sweeteners (OJ No L 61, p. 1).
21. British Pharmacopoeia Volume I & II Monographs: Medicinal and Pharmaceutical Substances Colloidal Anhydrous Silica.

22. Witasp, E., et al., *Efficient internalization of mesoporous silica particles of different sizes by primary human macrophages without impairment of macrophage clearance of apoptotic or antibody-opsonized target cells.* Toxicology and applied pharmacology, 2009. **239**(3): p. 306-319.
23. Vallhov, H., et al., *Mesoporous silica particles induce size dependent effects on human dendritic cells.* Nano Letters, 2007. **7**(12): p. 3576-3582.
24. Kupferschmidt, N., et al., *In vivo oral toxicological evaluation of mesoporous silica particles.* Nanomedicine, 2013. **8**(1): p. 57-64.
25. Fu, C., et al., *The absorption, distribution, excretion and toxicity of mesoporous silica nanoparticles in mice following different exposure routes.* Biomaterials, 2013. **34**(10): p. 2565-2575.
26. Lu, J., et al., *Biocompatibility, biodistribution, and drug-delivery efficiency of mesoporous silica nanoparticles for cancer therapy in animals.* Small, 2010. **6**(16): p. 1794-1805.
27. Hudson, S.P., et al., *The biocompatibility of mesoporous silicates.* Biomaterials, 2008. **29**(30): p. 4045-4055.
28. Yildirim, A., E. Ozgur, and M. Bayindir, *Impact of mesoporous silica nanoparticle surface functionality on hemolytic activity, thrombogenicity and non-specific protein adsorption.* Journal of Materials Chemistry B, 2013. **1**(14): p. 1909-1920.
29. Attard, G.S., J.C. Glyde, and C.G. Göltner, *Liquid-crystalline phases as templates for the synthesis of mesoporous silica.* Nature, 1995. **378**(6555): p. 366-368.
30. Firouzi, A., et al., *Cooperative organization of inorganic-surfactant and biomimetic assemblies,* Science, 1995. **267**:p24.
31. Chen, C.-Y., et al., *Studies on mesoporous materials II. Synthesis mechanism of MCM-41.* Microporous Materials, 1993. **2**(1): p. 27-34.
32. Alothman, Z.A., *A review: fundamental aspects of silicate mesoporous materials.* Materials, 2012. **5**(12): p. 2874-2902.
33. Bharti, C., et al., *Mesoporous silica nanoparticles in target drug delivery system: a review.* International journal of pharmaceutical investigation, 2015. **5**(3): p. 124.
34. Zhang, F., et al., *Understanding effect of wall structure on the hydrothermal stability of mesostructured silica SBA-15.* The Journal of Physical Chemistry B, 2005. **109**(18): p. 8723-8732.
35. Federiconi, F., et al., *How soft are biological helices? A measure of axial and lateral force constants in folate quadruplexes by high-pressure X-ray diffraction.* Eur Biophys J, 2011. **40**(11): p. 1225-35.
36. Gibson, L., *Mesosilica materials and organic pollutant adsorption: part A removal from air.* Chemical Society Reviews, 2014. **43**(15): p. 5163-5172.
37. Israelachvili, J.N., D.J. Mitchell, and B.W. Ninham, *Theory of self-assembly of hydrocarbon amphiphiles into micelles and bilayers.* Journal of the Chemical Society, Faraday Transactions 2: Molecular and Chemical Physics, 1976. **72**: p. 1525-1568.
38. Mehta, S. and G. Kaur, *Microemulsions: thermodynamic and dynamic properties*, in *Thermodynamics*. 2011, InTech.
39. Axelrod, J., *The pineal gland: a neurochemical transducer.* Science, 1974. **184**(4144): p. 1341-1348.
40. Klein, D.C. and R.Y. Moore, *Suprachiasmatic nucleus: the mind's clock*. 1991: Oxford University Press, USA.
41. Dibner, C., U. Schibler, and U. Albrecht, *The mammalian circadian timing system: organization and coordination of central and peripheral clocks.* Annual review of physiology, 2010. **72**: p. 517-549.
42. Vetter, C. and F.A. Scheer, *Circadian Biology: Uncoupling Human Body Clocks by Food Timing.* Current Biology, 2017. **27**(13): p. R656-R658.

43. Srinivasan, V., et al., *Melatonin and melatonergic drugs on sleep: possible mechanisms of action.* International Journal of Neuroscience, 2009. **119**(6): p. 821-846.
44. Touitou, Y., A. Reinberg, and D. Touitou, *Association between light at night, melatonin secretion, sleep deprivation, and the internal clock: Health impacts and mechanisms of circadian disruption.* Life Sciences, 2017.
45. Liu, J., et al., *MT1 and MT2 melatonin receptors: a therapeutic perspective.* Annual review of pharmacology and toxicology, 2016. **56**: p. 361-383.
46. Ferracioli-Oda, E., A. Qawasmi, and M.H. Bloch, *Meta-analysis: melatonin for the treatment of primary sleep disorders.* PloS one, 2013. **8**(5): p. e63773.
47. Saxvig, I.W., et al., *A randomized controlled trial with bright light and melatonin for delayed sleep phase disorder: effects on subjective and objective sleep.* Chronobiology international, 2014. **31**(1): p. 72-86.
48. Carrillo-Vico, A., et al., *A review of the multiple actions of melatonin on the immune system.* Endocrine, 2005. **27**(2): p. 189-200.
49. García-García, P., F. López-Muñoz, and C. Álamo, *New Galenic Formulations of Melatonin*, in *Melatonin, Neuroprotective Agents and Antidepressant Therapy*. 2016, Springer. p. 193-202.
50. Foley, D.J., et al., *Sleep complaints among elderly persons: an epidemiologic study of three communities.* Sleep: Journal of Sleep Research & Sleep Medicine, 1995.
51. Garbarino, S., et al., *Sleepiness and sleep disorders in shift workers: a study on a group of Italian police officers.* Sleep, 2002. **25**(6): p. 648-653.
52. Rutten, J., *Jet lag: symptoms, causation and minimization.* Maastricht Student Journal of Psychology and Neuroscience, 2016. **4**.
53. Mallo, C., et al., *Pharmacokinetics of melatonin in man after intravenous infusion and bolus injection.* European journal of clinical pharmacology, 1990. **38**(3): p. 297-301.
54. Dev, A., et al., *Critical aspects in sublingual route of drug delivery.* Pharmaceutical and Biological Evaluations, 2016. **3**(1): p. 42-49.
55. Dawson, D., et al., *Effect of sustained nocturnal transbuccal melatonin administration on sleep and temperature in elderly insomniacs.* Journal of biological rhythms, 1998. **13**(6): p. 532-538.
56. Kanikkannan, N., et al., *Formulation and in vitro evaluation of transdermal patches of melatonin.* Drug development and industrial pharmacy, 2004. **30**(2): p. 205-212.
57. Dubey, V., D. Mishra, and N. Jain, *Melatonin loaded ethanolic liposomes: physicochemical characterization and enhanced transdermal delivery.* European Journal of Pharmaceutics and Biopharmaceutics, 2007. **67**(2): p. 398-405.
58. Aeschbach, D., et al., *Use of transdermal melatonin delivery to improve sleep maintenance during daytime.* Clinical Pharmacology & Therapeutics, 2009. **86**(4): p. 378-382.
59. Mao, S., et al., *Intranasal administration of melatonin starch microspheres.* International Journal of Pharmaceutics, 2004. **272**(1): p. 37-43.
60. Zisapel, N., *Development of a melatonin-based formulation for the treatment of insomnia in the elderly.* Drug development research, 2000. **50**: p. 226-234.
61. Government, A., *Australian Public Assessment Report for Melatonin*, D.o.H.a. Ageing, Editor. 2009.
62. Elmore, S., *Apoptosis: a review of programmed cell death.* Toxicologic pathology, 2007. **35**(4): p. 495-516.
63. Koopman, G., et al., *Annexin V for flow cytometric detection of phosphatidylserine expression on B cells undergoing apoptosis.* Blood, 1994. **84**(5): p. 1415-1420.
64. Hancock, J., R. Desikan, and S. Neill, *Role of reactive oxygen species in cell signalling pathways*. 2001, Portland Press Limited.

65. Li, N., et al., *Mitochondrial complex I inhibitor rotenone induces apoptosis through enhancing mitochondrial reactive oxygen species production.* Journal of Biological Chemistry, 2003. **278**(10): p. 8516-8525.
66. Ryter, S.W., et al., *Mechanisms of cell death in oxidative stress.* Antioxidants & redox signaling, 2007. **9**(1): p. 49-89.
67. Schoeffel, M., et al., *Wall thickness determination of hydrophobically functionalized MCM-41 materials.* Journal of Materials Chemistry, 2012. **22**(2): p. 557-567.
68. Caminiti, R., et al., *Powder X-ray data for melatonin C 13 H 16 N 2 O 2.* Powder Diffraction, 2000. **15**(2): p. 108-111.
69. Carrott, M.R., et al., *Adsorption of nitrogen, neopentane, n-hexane, benzene and methanol for the evaluation of pore sizes in silica grades of MCM-41.* Microporous and mesoporous materials, 2001. **47**(2): p. 323-337.
70. Landers, J., G.Y. Gor, and A.V. Neimark, *Density functional theory methods for characterization of porous materials.* Colloids and Surfaces A: Physicochemical and Engineering Aspects, 2013. **437**: p. 3-32.
71. Huang, W.-C., et al., *Mercaptopropyl-functionalized helical mesoporous silica nanoparticles with c2mm symmetry: Cocondensation synthesis and structural transformation in the dilute solution of mixed cationic and nonionic surfactants.* Microporous and Mesoporous Materials, 2012. **151**: p. 411-417.
72. Thommes, M., et al., *Adsorption hysteresis of nitrogen and argon in pore networks and characterization of novel micro-and mesoporous silicas.* Langmuir, 2006. **22**(2): p. 756-764.
73. McNaught, A.D. and A.D. McNaught, *Compendium of chemical terminology*. Vol. 1669. 1997: Blackwell Science Oxford.

# Supporting Information

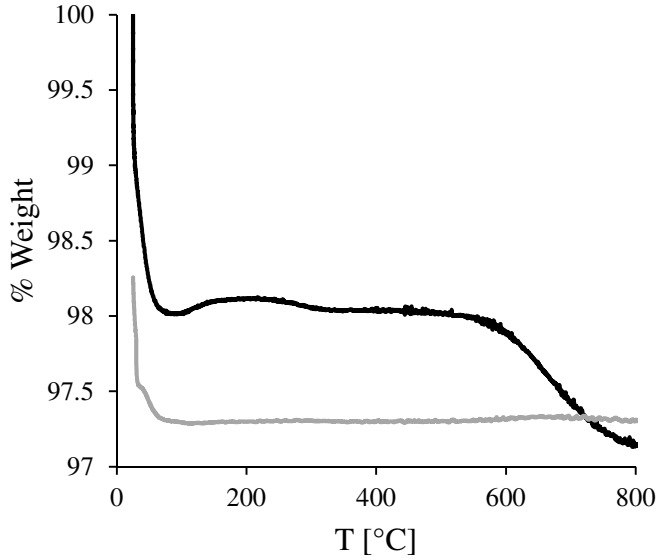


Figure 32. TGA curve of MCM-41: weight loss (black line) and its derivative (grey line) as a function of temperature showed an initial loss of solvent still present in the sample (1.9wt%) and then a weight loss of 1wt% that can be associated with the silica particles.

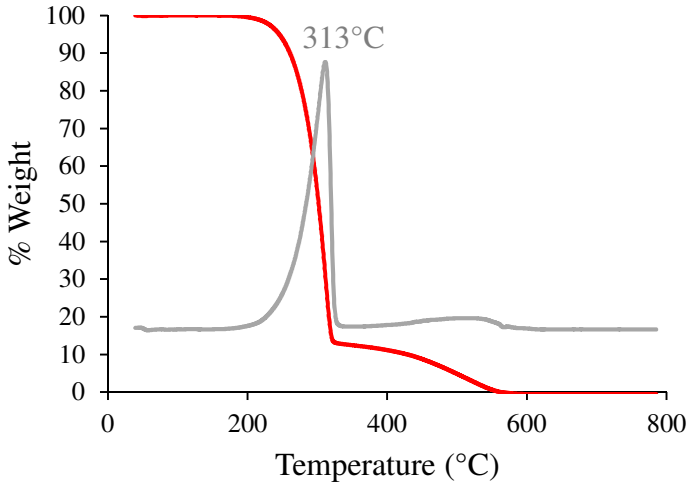


Figure 33. TGA curve of free melatonin: sample weight loss (red line) and its derivative (grey line) as a function of temperature. Melatonin decomposition is a two steps process with the main step between 226° and 326° C and the second between 448° and 558° C.

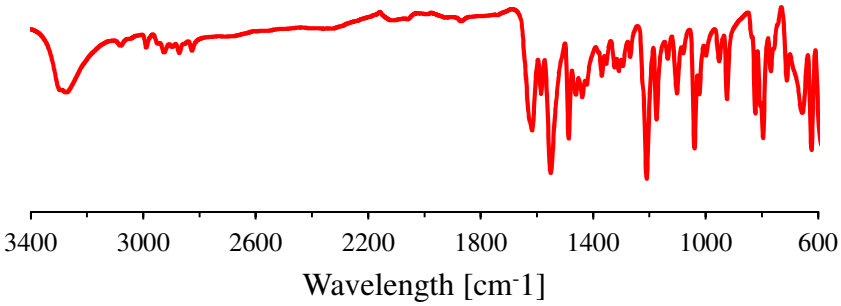


Figure 34. FT-IR of free melatonin presented peaks at 3290, 1620 and 1210 $cm^{-1}$ which can be associated with N-H stretch, C=O and C-N respectively.

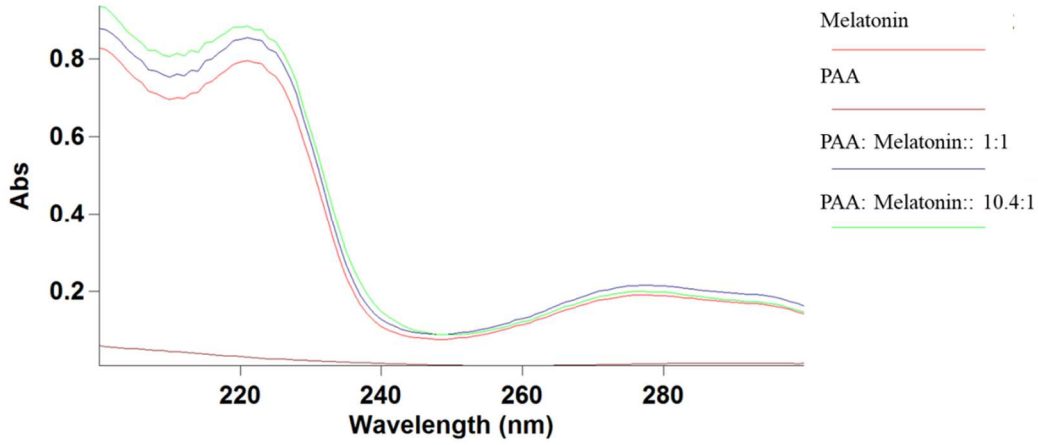


Figure 35. UV-Vis scan of melatonin and PAA at neutral pH shows two peaks: one around 221 nm and the other around 277 nm. The main peak is the one at 221 nm. At this wavelength melatonin has an absorbance of 0.797 and PAA alone shows no peaks. When PAA and melatonin are present together in the sample, the absorbance at 221 nm increases up to 0.885 if the ratio PAA: melatonin is 10.4:1 (which is the ratio between PAA and melatonin in the formulation designed in this project).

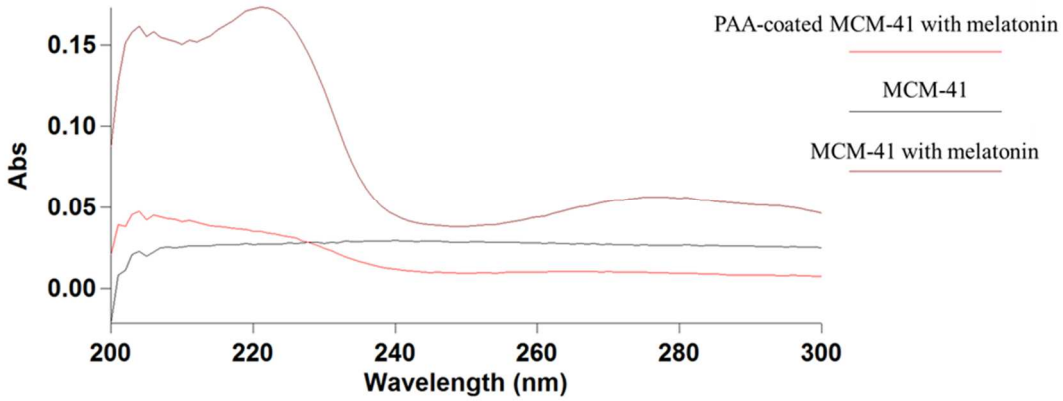


Figure 36. UV-Vis scan in the wavelength range 200 – 300 nm of MCM-41, MCM-41 with melatonin and PAA-coated MCM-41 with melatonin in SGF (pH 1.2). MCM-41 did not seem to affect melatonin absorbance.

b

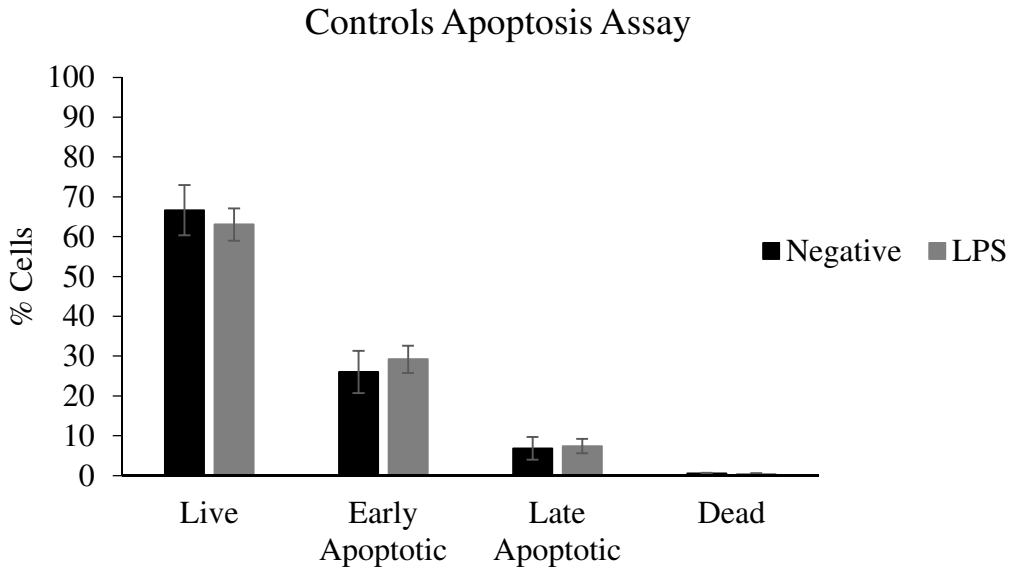


Figure 37. No statistically significant difference was assessed between the negative and positive (LPS) controls. LPS did not affect cells viability as expected.

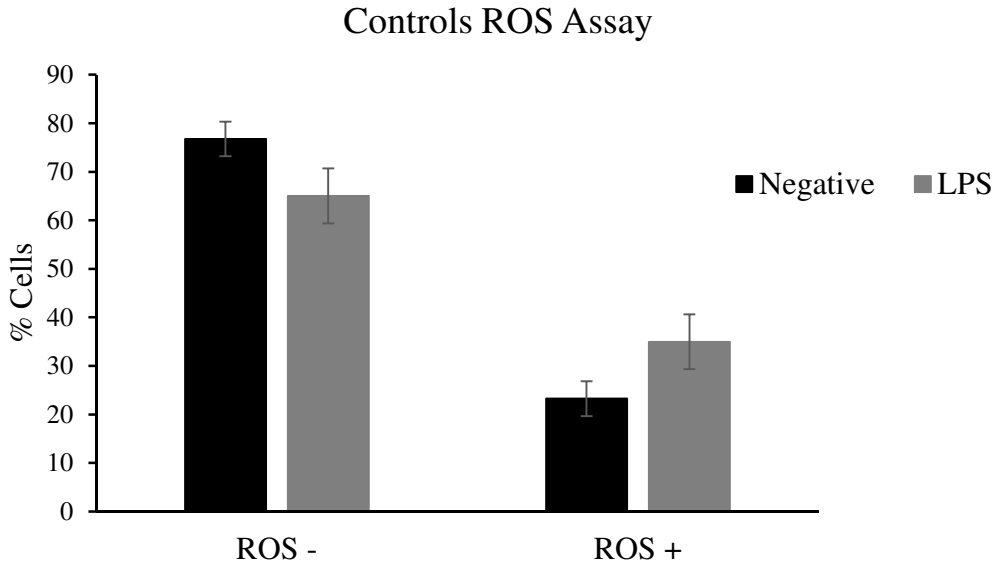


Figure 38. LPS (positive control) did not significantly affected the percentage of ROS positive cells in comparison to the negative control.

c